Review of Morphing Laminated Composites

V. S. C. Chillara[1]
NSF IUCRC on Smart Vehicle Concepts,
Department of Mechanical and
Aerospace Engineering,
The Ohio State University,
Columbus, OH 43210
e-mail: chillara.1@osu.edu

M. J. Dapino
NSF IUCRC on Smart Vehicle Concepts,
Department of Mechanical and
Aerospace Engineering,
The Ohio State University,
Columbus, OH 43210
e-mail: dapino.1@osu.edu

Morphing structures, defined as body panels that are capable of a drastic autonomous shape transformation, have gained importance in the aerospace, automotive, and soft robotics industries since they address the need to switch between shapes for optimal performance over the range of operation. Laminated composites are attractive for morphing because multiple laminae, each serving a specific function, can be combined to address multiple functional requirements such as shape transformation, structural integrity, safety, aerodynamic performance, and minimal actuation energy. This paper presents a review of laminated composite designs for morphing structures. The trends in morphing composites research are outlined and the literature on laminated composites is categorized based on deformation modes and multifunctional approaches. Materials commonly used in morphing structures are classified based on their properties. Composite designs for various morphing modes such as stretching, flexure, and folding are summarized and their performance is compared. Based on the literature, the laminae in an n-layered composite are classified based on function into three types: constraining, adaptive, and prestressed. A general analytical modeling framework is presented for composites comprising the three types of functional laminae. Modeling developments for each morphing mode and for actuation using smart material-based active layers are discussed. Results, presented for each deformation mode, indicate that the analytical modeling can not only provide insight into the structure's mechanics but also serve as a guide for geometric design and material selection. [DOI: 10.1115/1.4044269]

Keywords: morphing, laminated composites, multifunctional, analytical model, bistable, curvature, stretching, folding, actuation

1 Background

1.1 Definition. This paper is a review of multifunctional laminated composites that are applicable to morphing structures. The terms that define the scope of this review are explained in Secs. 1.1.1 and 1.1.2.

1.1.1 Morphing Structures. Morphing structures undergo significant deformations in response to actuation relative to their characteristic dimensions in the unactuated state. The large deformations associated with morphing can be in the form of stretching of membranes, flexural deformation in thin plates, or folding at creases. Actuation for morphing is realized through an external force field or through embedded active materials that respond to an external stimulus. Some flora and fauna possess morphing abilities that enable a specific set of needs to be fulfilled in each shape. For example, birds adjust wing morphology to optimize performance in various stages of flight such as take-off, cruising, and landing [1]. Plants such as the Venus fly trap engulf their prey by snapping their leaves together from an open state [2]. Naturally occurring morphing events can be gradual or discontinuous, and are typically self-actuated, which means that the forces are applied from within the structure. These ideas have inspired engineering applications such as morphing aircraft [3,4] and automobiles [5], and soft robotics [6,7].

1.1.2 Multifunctional Laminated Composites. Laminated composites are a construct in which materials, in the form of sheets or plies, are stacked together as layers to achieve material properties that are superior to those of the individual materials. The mechanics of laminated composites is influenced by the dimensions, orientation, and material properties of each of the constituent laminae. The stiffness of passive composites can be tailored to facilitate mechanics such as stretching, flexure, or folding. However, large deformation is associated with tradeoffs in the stiffness to operational loads and actuation work [5]. These tradeoffs can be addressed using smart materials such as piezoelectrics, shape memory alloys (SMA), and active polymers. Smart composites, for example, can be softened to enhance the morphing range with minimal actuation effort and can be stiffened to withstand operational loads with minimal shape deformation. Material systems comprising laminae that are tailored to serve functions such as structural integrity, built-in actuation, intrinsic morphing features (such as bistability), and variable stiffness are defined in this review as multifunctional laminated composites.

1.2 Trends in Morphing Laminated Composites. Interest in the field of morphing structures has grown exponentially in the past two decades (1997–2017). Based on the count returned by the search engine *Google Scholar*, the number of publications, excluding patents, in the field of *composite*-based *morphing* structures are an order of magnitude lower than in *morphing structures* in general. Also, publications related to morphing *laminates* or *laminated composites* are an order of magnitude fewer than *morphing composites*. The compounded average growth rate for research on morphing structures, composites, and laminates is calculated to be 11%, 14.94%, and 18.59% respectively, highlighting the attractiveness of laminated composites for morphing. The increasing number of patents at a compounded rate of 17.2% in the last two decades indicates growing interest in the adoption of morphing laminates for commercial applications.

1.3 Morphing Applications. Applications that benefit from shape adaptive structures are discussed in this subsection. The emphasis is on aircraft and automobiles where morphing panels enable optimal aerodynamic performance for improved fuel

[1]Corresponding author.

Manuscript received December 14, 2018; final manuscript received July 8, 2019; published online October 30, 2019. Assoc. Editor: Rui Huang.

economy. Other applications include morphing wind turbine blades, soft robotics, and deployable space structures.

1.3.1 Aircraft. Morphing aircraft have received significant attention in recent decades due to the potential for increasing fuel economy and reducing emissions in commercial aircraft, and developing multirole aircraft for defense operations [8]. Bowman et al. [9] numerically evaluated the benefits of morphing the planform shape and profile of the wings of an aircraft. Several wing concepts have been developed with the goal of morphing the span, sweep, wing twist, airfoil camber, and spanwise bending. These developments have been reviewed extensively by Thill et al. [10], Sofla et al. [11], Barbarino et al. [3], and Weisshaar [12]. The ideal morphing configuration for the wings depends on the type of aircraft (commercial, military, cargo, etc.) and its operating requirements such as flight range, payload, speed, and agility.

Examples of laminated structures that have been investigated for aircraft wing morphing include: SMA-reinforced soft composites whose curvature is controlled by actuating the SMAs [13,14] (Fig. 1(*a*)); corrugated composites [15] with passive and shape memory polymer (SMP) layers [16] that can fix their deformed shape and recover their initial shape (Fig. 1(*b*)); piezoelectric macrofiber composites (MFC) as laminar actuators for controlling the curvature of a passive structure [17,18]; bistable composites with curvature [19], tailored twist [20], and zero torsional stiffness [21] for morphing between two stable shapes; composite lattice-based cellular structures [22] (Fig. 1(*c*)), and hybrid laminated composites with high spanwise stiffness and localized low flexural stiffness [23,24](Fig. 1(*d*)). Devices based on bistable composites have been developed for air flow control [25,26]. Sun et al. [27] reviewed smart material-based sensors, actuators, structures, and controllers for morphing aircraft.

1.3.2 Automobiles. Aerodynamic drag increases parabolically with an increase in vehicle speed. Drag can be minimized by morphing the vehicle body into the optimal shape at a given speed. A 10% reduction in aerodynamic drag yields a 2% increase in fuel economy [28]. At low speeds, where aerodynamic performance is not critical, morphing panels enhance exterior styling, thermal efficiency, crashworthiness, etc. [29]. Hucho [30] summarized various geometric modifications to the vehicle body that reduce drag. Examples of morphing structures that serve as drag-reducing features include: boat-tail extension [31]; vortex generators [32]; morphing fender skirts [33]; active radiator grills [34]; active underbody cover [35]; deployable side mirrors [30]; deployable air dam [36]; and rear diffuser with a controllable angle of attack [34].

Daynes and Weaver reviewed morphing structure concepts for automobiles up to the year of 2013 [5]. Some of the key morphing vehicle concepts presented since 2013 are: morphing fender on the BMW Next 100 Years concept [37]; boat-tail extension on the Mercedes Benz Intelligent Aerodynamic Automobile concept [38]; inflatable front spoiler on a Porsche 911 Turbo S [39]; and active flaps for engine thermal management on a Ferrari 458 Speciale [40]. Chillara et al. [41] demonstrated a self-supported and self-actuated morphing fender skirt that is dome-shaped at low speed and flattens at high speed (Fig. 2(*a*)); flattening in curved prestressed composites is realized through laminar SMA wires that contract on heating. SMAs have also been employed to control the curvature of a soft composite-based rear spoiler [42] (Fig. 2(*b*)). Spiteri et al. [43] developed a bistable origami-folded ram-air intake system for automotive engines. Qamar et al. [44] reviewed materials for human computer interaction that may be applicable to reconfigurable interiors in automobiles. Overall, the number of publications on morphing composites is far fewer for automobiles than compared to aircraft.

1.3.3 Other Applications. The cost of wind energy can be lowered by increasing the generating capacity of wind turbines. Power output can be amplified by increasing rotor diameter but at the cost of higher aerodynamic loads at the blade roots and higher inertial loading. Aeroelastic tailoring of rotor blades is an

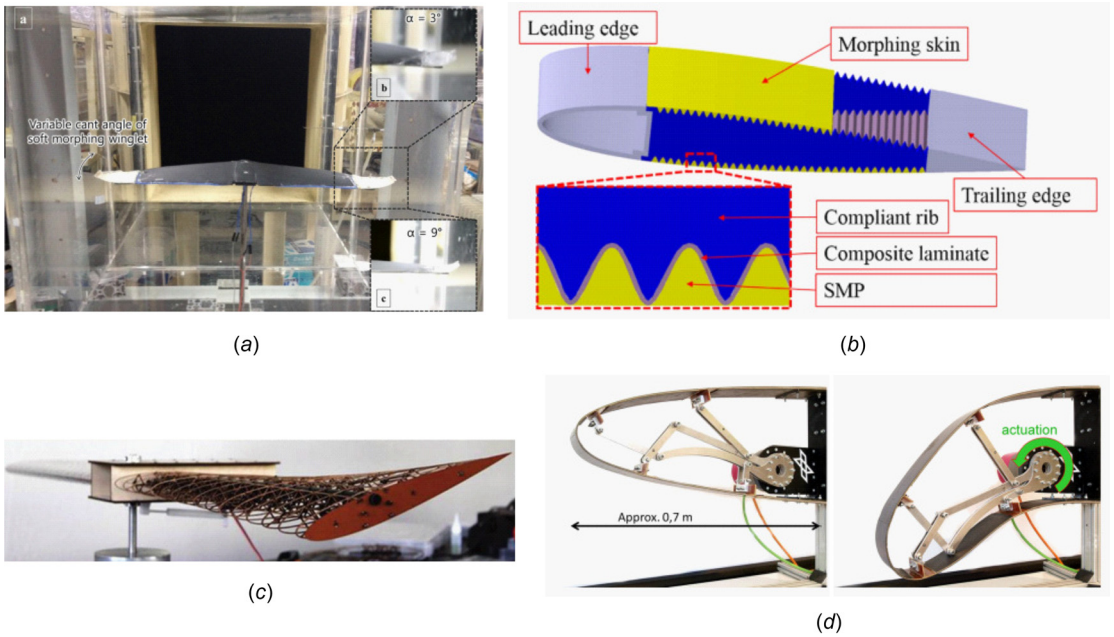

(*a*) (*b*) (*c*) (*d*)

Fig. 1 Composite structures in morphing aircraft wings: (*a*) unmanned aerial vehicle with SMA-actuated soft morphing winglets (reproduced with permission from Han et al. [14]. Copyright 2016 by Elsevier Ltd.), (*b*) variable camber wing based on a smart composite comprising corrugations filled with SMP (reproduced with permission from Gong et al. [16]. Copyright 2017 by IOP Publishing), (*c*) twisting wing based on cellular structures laminated to a flexible skin (reproduced with permission from Jenett et al. [22]. Copyright 2017 by Mary Ann Liebert Inc.), and (*d*) droop-nose demonstrator based on a hybrid composite skin comprising localized soft regions for flexure (reproduced with permission from Rudenko et al. [23]. Copyright 2017 by SAGE Publications).

Fig. 2 (*a*) Morphing fender skirt concept based on SMA-actuated prestressed composites [41] and (*b*) a morphing rear spoiler made of woven SMA-driven soft composites (reproduced with permission from Han et al. [42]. Copyright 2016 by Elsevier Ltd.)

attractive approach for maximizing power and durability. Lightweight blades with tailored stiffness have low inertial loads and can generate power up to a critical aerodynamic load beyond which they morph into nonfunctional shapes, thereby alleviating stress and improving durability. Lachenal et al. [45] reviewed morphing composite-based structures for wind turbine blades. Commonly studied methods for load alleviation are based on tailoring the bend-twist coupling of a composite blade. They include: multimaterial structures with variable ply thickness [46] and selective stiffeners [47]; and composites with variable stiffness that exhibit multistability [48], zero torsional stiffness [21] (Fig. 3(*a*)), and active shape change using embedded SMA actuators [49,50].

Soft robots are perceived as robots whose shape and stiffness can be controlled to realize locomotion, safety in human–robot interaction, and dexterous activities like gripping objects and moving them. Composite-based designs of soft robots typically include active materials that are embedded in or laminated to passive layers [51]. Locomotion is achieved by controlling the input to the active material to create flexure or folding in the body [52,53] (Fig. 3(*b*)). Stiffness control is critical in human–robot interaction where the robot is expected to soften when it comes in contact with a human. Manti et al. [54] reviewed stiffening mechanisms, some of which are relevant in a laminated composites construct. Li and Wang [55] reviewed plant inspired adaptive structures and materials for morphing. Examples of bioinspired composite structures include: a starfish robot based on embedded SMA wire actuators [56]; jellyfish robot based on ionic polymer metal composite actuators [57]; inchworm-inspired robot and turtle-like swimming robot made of smart soft composite [58,59] (Fig. 3(*c*)); and fluid-actuated elastomeric robots [60]. Cao et al. [52] presented untethered soft robots that are actuated using soft electrostatic actuators.

Deployable structures are attractive for aerospace applications because they can be packaged in a small volume during launch

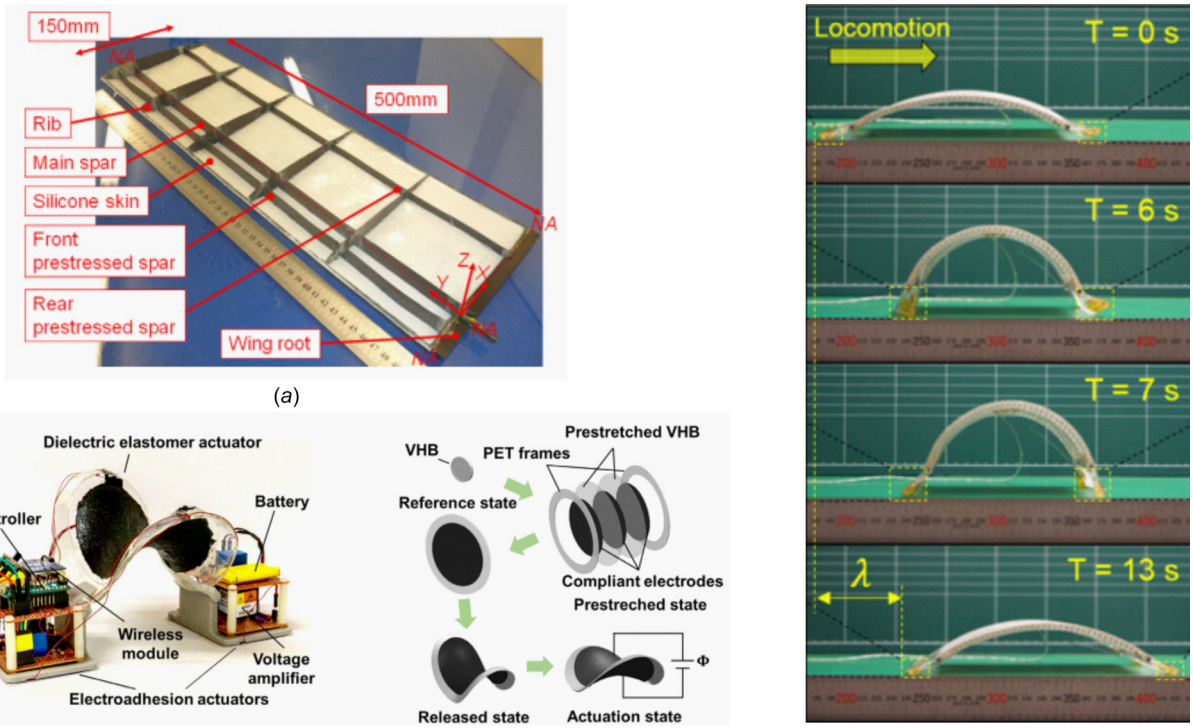

Fig. 3 (*a*) Morphing wing with zero torsional stiffness (reproduced with permission from Daynes et al. [21]. Copyright 2015 by Elsevier Ltd.), (*b*) untethered soft robot based on a dielectric elastomeric actuator (reproduced with permission from Cao et al. [45]. Copyright 2018 by Elsevier Ltd.), and (*c*) inchworm-inspired robot made of soft composites with embedded SMA wire actuators (reproduced with permission from Wang et al. [46]. Copyright by IOP Publishing).

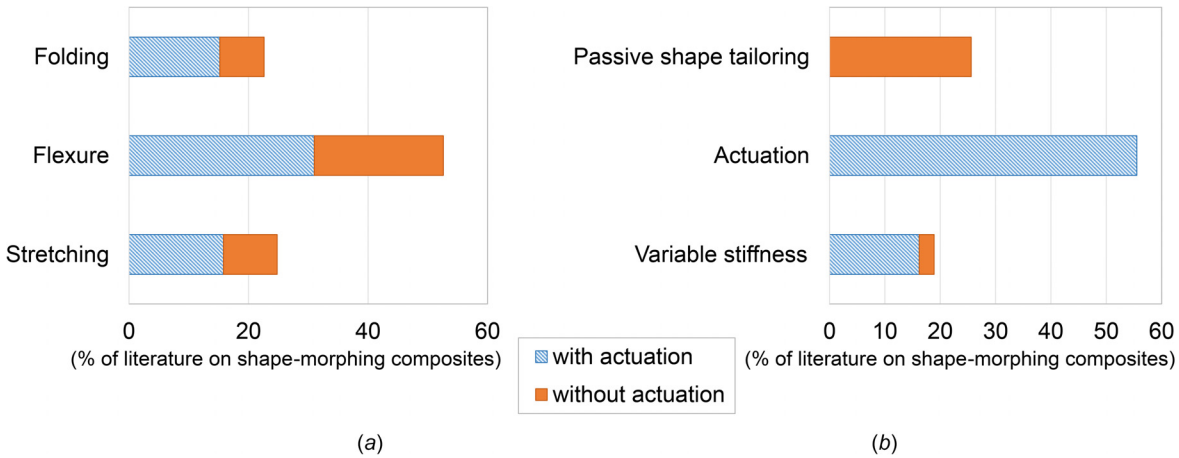

Fig. 4 Categorization of 2300 publications on morphing laminated composites from 1997 to 2017 based on a *Google Scholar* search. Trends related to: (*a*) deformation modes and (*b*) multifunctional designs.

and can be deployed over a large area when in orbit. Examples include solar arrays and boom structures [61]. Fiber-reinforced shape memory polymeric composites are attractive because they can be folded or rolled in one configuration and can be opened or flattened when heated. These materials have been developed under the name of elastic memory composites [62]. Wang et al. [63] developed truss-like structures based on composites with soft elastomeric hinges that are actuated by shape memory alloy wires. Bistable composite tape-springs can be deployed from a rolled-up bulk state into a boom structure [64,65].

1.4 Classification of Morphing Laminated Composites. Laminated composites developed for morphing structures are categorized based on a keyword search as shown in Fig. 4. A comparison of deformation modes of the laminates shows that flexure, including twisting and coiling, has been studied the most (Fig. 4(*a*)). Interest in special features such as multistability and embedded actuation has contributed to this trend. Figure 4(*b*) shows that more than half of the work on morphing laminates includes the notion of actuation. The rest of the literature is on identifying new material combinations for morphing and tailoring the anisotropy of passive composites. Our literature search on *variable stiffness* included passive composites with functionally graded stiffness and active composites that can change their stiffness on command. Results show that there has been relatively little work on variable stiffness structures compared to actuation. In Sec. 2, various active and passive materials that have been used in the design of morphing laminated composites are summarized and the rationale behind their selection is discussed.

2 Materials for Morphing Composites

The choice of materials for a given morphing mode depends on material modulus, strain capability, and anisotropy. The upper limits of Young's modulus and usable strain of various passive and active materials commonly used in morphing composites are shown in Fig. 5. Soft materials with high strain capability are candidates for stretchable membranes or skins. Kikuta [66] compared various stretchable material candidates including elastomers such as silicone rubber and polyurethanes, copolyesters, and woven fabrics such as Spandex. These materials are capable of strain on the order of 100%. Among the materials evaluated, silicone rubber has the highest strain capability, minimal residual strain on unloading, and can be used as a matrix material in reinforced composites.

Anisotropy in stretchable materials can be tailored to achieve a target magnitude and direction of strain and stiffness. For example, stretching in an elastomer can be confined to one direction by reinforcing the material with unidirectional fibers such as carbon or aramid in a direction orthogonal to the stretched direction. Such fiber-reinforced elastomers, also known as elastomeric matrix composites (EMC), exhibit near-zero in-plane Poisson's ratio due to the restriction offered by the fibers [67,68]. The out-of-plane stiffness of EMC membranes can be augmented by applying prestress in the fiber-direction; it is often a structural requirement that the out-of-plane stiffness of stretchable skins be high. Besides enabling changes in surface area, stretchable skins provide restoring forces that aid flexure and folding when installed in a prestressed configuration [69,70].

Ductile materials that have high modulus and low strain relative to elastomers can be used as laminae that provide structural integrity to the composite. These laminae have high in-plane stiffness to restrict stretching but low out-of-plane stiffness to enable flexure. For example, thin sheets of isotropic materials such as steel, aluminum, and nylon can be paired with an active layer that shrinks or expands to create a smooth curvature in the composite [41,70,71]. Brittle materials such as epoxy-based polymers can be reinforced with fibers to create thin composites for morphing. When cured at elevated temperatures, these fiber-reinforced polymeric composites (FRP) can exhibit multiple stable curved shapes at room temperature, depending on the composite's geometry, fiber-orientation, and curing temperature [72–74].

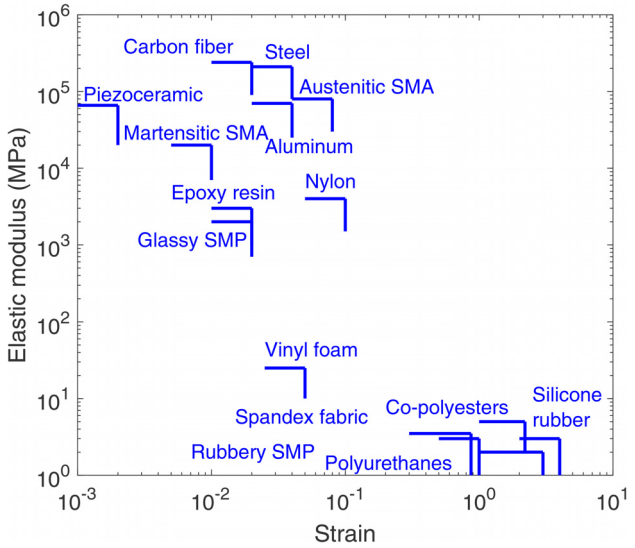

Fig. 5 Materials commonly used in morphing laminated composites

Table 1 Summary of stretchable laminated composites

Feature	Actuation source	Strain capability	Actuation energy density[a] (kJ/m^3)	Flexural stiffness[b] (MPa/m)	Advantages (■) and limitations (□)
EMCs [67,79,80]	External force	> 100%	1.25	0.147	■ Zero Poisson's ratio for 1D morphing ■ Tailorable fiber distribution □ Low out-of-plane stiffness □ Require support structure
Elastomer bonded to cellular support layer [68]	External force	> 100%	0.535	4.8	■ Higher out-of-plane stiffness than pure skin □ Higher actuation energy than pure skin
Honeycombs sandwiched between stretchable laminae [81–84]	External force	Up to 12 times material limit	1130	16.3	■ High out-of-plane stiffness ■ Potential for nonuniform stretching through functionally graded cells □ Penalty on composite thickness
Compliant laminae with sandwiched corrugations [85–88]	External force	10%	52	0.289	■ Corrugations amplify out-of-plane stiffness ■ Can program upper limit on strain ■ Can exhibit bilinear in-plane stiffness □ Penalty on the composites' thickness
Made of semicircular Corrugations [87]		2 × feature radius	N/A (along feature) 77 (orthogonal)	15,400 3.9	
Fluid channels embedded in compliant media [77,89–91]	Pressurized fluid	Up to 20%	2.5 (with trapped fluid), 0.1 (variable fluid volume)	50	■ Controllable strain ■ Controllable stiffness □ Fluid power sources can be bulky
Fiber reinforcement in SMPs [92–95]	Resistive heating	5% (glassy) >100% (rubbery)	1160 19.5	1.4 0.043	■ Shape fixity ■ Shape memory □ Actuation response is slow

[a]Strain energy per unit volume at 10% uniaxial strain.
[b]Stiffness of an Euler-Bernoulli beam subjected to a uniformly distributed load.
N/A—not available.

Materials whose stress-states can be controlled using external inputs such as heat, electric field, and light are termed smart materials. When paired with passive layers, smart laminae can create a strain mismatch that leads to flexure or folding. Piezoceramics can generate up to 0.2% strain in response to an applied voltage [75]. These ceramics are commercially available in the form of flexible laminae as piezoelectric MFC. For large deflections, SMA provide sufficient strain capability (up to 8%) to serve as embedded actuators. SMAs transform from their detwinned Martensite phase to the Austenite phase when heated beyond their transformation temperature at a given stress state. SMPs exist in their respective rubbery and glassy states above and below their glass transition temperature (T_g). SMPs can undergo a strain of up to 400% in their rubbery state. The strain can be fixed by cooling the SMP below T_g and can be recovered by heating the material back above T_g. Smart laminae can also be realized through fluid channels created in compliant materials. Stretching and flexure can be achieved by modulating fluid pressure [76], whereas stiffness can be controlled by trapping the fluid in the adaptive layer [77,78].

3 Deformation Modes of Morphing Composites

Methods to achieve various morphing modes such as stretching, flexure, and folding, are reviewed in this section. The laminae in a generic composite are classified based on function as constraining, stress-biased, and adaptive. A constraining layer has high in-plane modulus relative to the other laminae and serves to augment out-of-plane deformation while suppressing in-plane strain. Examples include isotropic sheets made of metals and plastics as well as anisotropic flexible material systems such as FRP laminates, corrugated structures, and cellular structures. A stress-biased layer is a source for an intrinsic restoring force that provides shape bias at equilibrium. This layer is made of stretchable materials such as elastomers and shape memory polymers. An adaptive layer is an active material whose stress-state can be modulated to control the shape and stiffness of the composite. Examples include SMAs, SMPs, pressurizable fluid channels or fluidic layers, parrafin wax, magnetorheological foam, etc. The three types of laminae constitute a framework for designing large deformations for morphing.

3.1 Stretching. Stretchable composites are material systems that provide a change in surface area. The requirement for stretchable morphing systems is to have low in-plane stiffness but high out-of-plane stiffness. Various designs of stretchable composites are summarized in Table 1. Fiber-reinforcement of elastomers is a versatile approach for the tailoring of stretchable features in membranes. Murray et al. [67] developed zero-Poisson's ratio elastomers by reinforcing the matrix with unidirectional fibers in the direction orthogonal to the morphing direction. Bubert et al. [68] improved the out-of-plane stiffness of these membranes by reinforcing them with a zero Poisson's ratio honeycomb (Fig. 6(*a*)). Fibers in a stretchable matrix can be functionally distributed to achieve a texture when the membrane is inflated [91] (Fig. 6(*b*)). Geometric features such as corrugations enable low in-plane stiffness in one direction and high bending stiffness in one or two directions [86] (Fig. 6(*c*)). Active elements such as pneumatic muscle fibers have been installed in a stretchable skin to control the strain of the composite [90] (Fig. 6(*d*)). When used in conjunction with valves, these muscles can also provide stiffness control [77]. Smart materials such as shape memory polymers are stiff in their glassy state and stretchable up to 400% in their rubbery state [96]. The strain in these polymers can be fixed by cooling them below their glass transition temperature in the stretched shape and

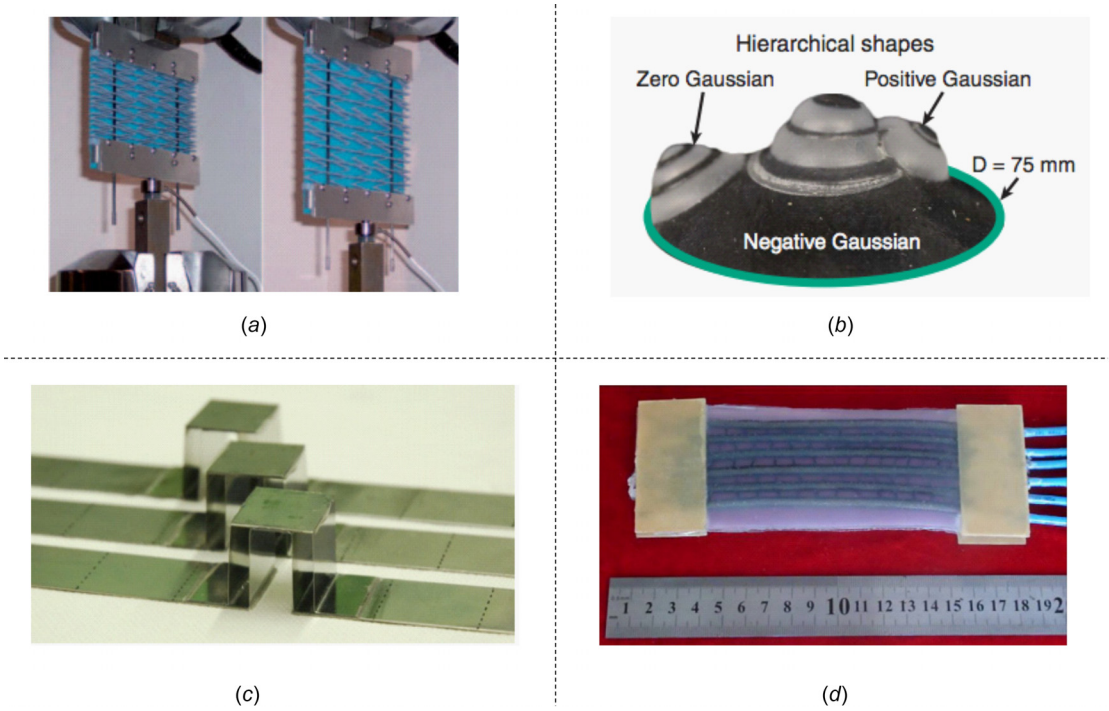

Fig. 6 (*a*) Composite with zero in-plane Poisson's ratio comprising fiber-reinforced elastomers bonded to a flexurally stiff honeycomb layer (reproduced with permission from Bubert et al. [68]. Copyright 2010 by SAGE Publications), (*b*) pneumatically actuated mesh-reinforced elastomer for texturing in stretchable surfaces (reproduced with permission from Pikul et al. [91]. Copyright 2017 by AAAS), (*c*) double-walled corrugated composite structures for stretchable surfaces with high bending stiffness (reproduced with permission from Previtali et al. [86]. Copyright 2014 by SAGE Publications), and (*d*) elastomeric composite embedded with pneumatic muscle fibers for controllable strain (reproduced with permission from Chen et al. [90]. Copyright 2011 by IOP Publishing).

can be recovered by heating them beyond the transition temperature.

3.2 Flexure. Flexible smart composites can be realized by combining a compliant active layer with controllable strain to a flexible but inextensible layer. Designs for flexural laminates are summarized in Table 2. Corrugations can be used to create composites with bilinear flexural stiffness that is characterized by the contact between corrugated unit cells [97]. Prior to contact between the unit cells, flexural stiffness is a function of cell geometry, whereas after contact, it is a function of the material properties of the composite. Cellular structures with tailored Poisson's ratio have been developed to create flexure configurations such as synclastic, anticlastic, and cylindrical curvatures. An example of a cylindrical composite based on shape memory polymers reinforced with zero-Poisson's ratio cellular structures is shown in Fig. 7(*a*). Smart flexible skins can be created by installing an active material at an offset from the neutral axis; an example of a flexible skin with SMAs fused to the matrix is shown in Fig. 7(*b*). Initially curved composites can be created by incorporating residual stress through thermal [72] or mechanical [70] means; Daynes and Weaver reviewed methods for applying prestress to composite structures [127]. The curved structure can be flattened using active laminae such as fluid channels as shown in Fig. 7(*c*); when actuation is turned off, the composite returns to its curved shape due to the intrinsic restoring stress.

The most commonly studied bistable composites are FRP laminates that are cured at an elevated temperature [128]. Residual stress develops due to the mismatch in thermal contraction between the matrix and the fiber. In laminates with an unsymmetric fiber lay-up, the resulting cylindrical curvatures have nonparallel axes. Daynes et al. [117] developed bistable laminates with symmetric curved shapes by applying prestress to the fibers during the curing process (Fig. 7(*d*)). Methods for amplifying the magnitudes of the bistable shapes include the sandwiching of metallic laminae with FRP laminae [71,115]. Chillara and Dapino [124,125] developed bistable laminates that are mechanically prestressed by bonding stretched fiber-reinforced elastomeric laminae on opposite faces of an inextensible lamina (Fig. 7(*e*)). The stable curved shapes are weakly coupled when the prestressed laminae are orthogonal to each other. A key difference between the stress-bias and thermal-curing mechanisms is that mechanical prestress can be applied locally whereas thermal stress is applied globally. Localization of prestress enables the inclusion of multifunctional laminae in the composite. Methods for the actuation of bistable composites include the use of smart laminae such as piezoelectric MFC [129], shape memory alloys [118,126], and thermal loading [119].

3.3 Folding. Foldable thick composites can be created by incorporating low flexural stiffness in a localized region that defines a crease. The modulus and/or thickness of the crease is much lower than that of its faces. Lang et al. [130] reviewed various techniques for thickness accommodation in origami-folded structures. Various mechanisms for foldable composites are summarized in Table 3. Folded composites can be categorized as: structures with zero-width creases and structures with finite-width creases. Zero-width creases yield sharp folds that can be created using paper or mold-cured materials whereas finite-width creases yield folds that have high localized curvature. Boncheva and Whitesides [132] developed sealed elastomer-coated origami paper structures that can be deployed through pneumatic inflation (Fig. 8(*a*)). Sharp creases can be obtained by curing laminae using materials such as silicone rubber in molds made in the folded shape. Daynes et al. [134] demonstrated multistable origami shapes using elastomeric laminae that have acrylonitrile butadiene

Table 2 Summary of flexible laminated composites

Feature	Actuation source	Actuation work density[a] (kJ/m^3)	Flexural stiffness[b] (kN/m)	Advantages (■) and limitations (□)
Corrugated CFRP laminates [97,98]	External force	35.68 (longitudinal) 0.0052 (transverse)	0.0143 (longitudinal) 2.1×10^{-6} (transverse)	■ Anisotropy enables flexure about one axis ■ Flexural stiffness is amplified when corrugations contact each other □ Flexure range is limited by feature geometry
CFRP corrugations filled with SMP [16]	Thermal loading	22,200 (glassy) 20,400 (rubbery)	236.1 (glassy), 216.6 (rubbery)	■ SMP filler provides smooth outer surface ■ Shape fixity
Composites with intrinsic fluid channels [70,99–101]	Pressurized fluid	26.1	1.51	■ Controllable shape and stiffness ■ Can be actuated using nastic approaches
Inflatable bistable cellular structures [102,103]	Pressurized fluid	30	10	■ Compatible with nastic actuation □ Thickness change during actuation
End-constrained SMA wires in embedded channels [41,56,104–107]	Resistive heating of SMAs	9300	38.54	■ Large force and stroke □ Low actuation speed
Embedded SMA wires fused to the matrix [107,108]		2230 (below A_f), 9446 (above A_f)	3.28 (below A_f), 13.85 (above A_f)	■ Switchable stiffness
SMP layer/matrix [109,110]	External force and resistive heating of SMP, SMA	24.34 (at 15°C), 0.649 (at 35°C)	0.75 (at 15°C), 0.02 (at 35°C)	■ Shape fixity and memory □ Low actuation speed □ Creep deformation
Composites with fibers Interleaved with thermoplastics [111–114]	Thermal loading	2410 (glassy), 1074 (rubbery)	3.6 (glassy), 1.6 (rubbery)	■ Simplicity in actuation □ Requires external force to reset shape
Bistable curvatures due to Thermally induced prestress [71,115–117]	External force, resistive heating of SMAs [118] thermal loading, [119] voltage applied to piezoelectric laminae [120–123]	17.21	0.077	■ Actuation required only to switch shapes ■ Rapid shape change post snap-through ■ Drastic shape changes are possible □ Sensitive to hygrothermal variations □ Sensitive to manufacturing inaccuracy □ Challenging to embed active laminae
Bistable curvatures due to mechanically induced prestress [124,125]	External force resistive heating of SMAs [126]	9.75	0.09	■ Weakly coupled shapes enable individual shape tailoring ■ Not intrinsically sensitive to hygrothermal variations ■ Localized prestress enables the addition of multifunctional laminae

[a]Actuation force per unit change in curvature per unit volume.
[b]Stiffness of an Euler-Bernoulli beam subjected to a three-point bend test.

styrene-reinforced faces (Fig. 8(*b*)). Premade origami sheets can be laminated with a sandwiched fluidic layer to create origami structures that have controllable shape and stiffness [78].

Folds in a laminate with constraining and active layers can be actuated using mechanisms similar to those described in flexible composites; the in-plane strain of an active material is controlled to create folds. Peraza-Hernandez et al. [141] developed self-folding structures whose creases can be reprogrammed through localized heating of an embedded SMA film/mesh. Felton et al. [147] created bimorph actuators that include precreased paper and SMPs that are activated using resistive heating (Fig. 8(*c*)). The folded shape can be fixed and recovered by cooling and reheating the SMP past the glass transition temperature. Self-folding approaches based on smart materials can be enhanced by including residual stress in the composite. For example, mechanical prestress in one of the laminae can yield a given folded shape, provide structural integrity, and serve as a internal spring that can not only restore the actuator's initial configuration but also minimize its power requirements. Chillara and Dapino [133] developed stress-biased laminated composites that have a folded equilibrium shape (Fig. 8(*d*)). These composites can be actuated using active laminae such as fluidic layers or through passive means such as a pair of external forces; the creases need not be actuated individually.

4 Modeling Methods

The theory underlying various morphing structure concepts is summarized in this section. In Sec. 4.1, we present a generic analytical modeling framework for thin plates (2D structures) based on classical laminate theory. Conditions of plane-stress and strain are assumed and the variations in thickness and through-thickness

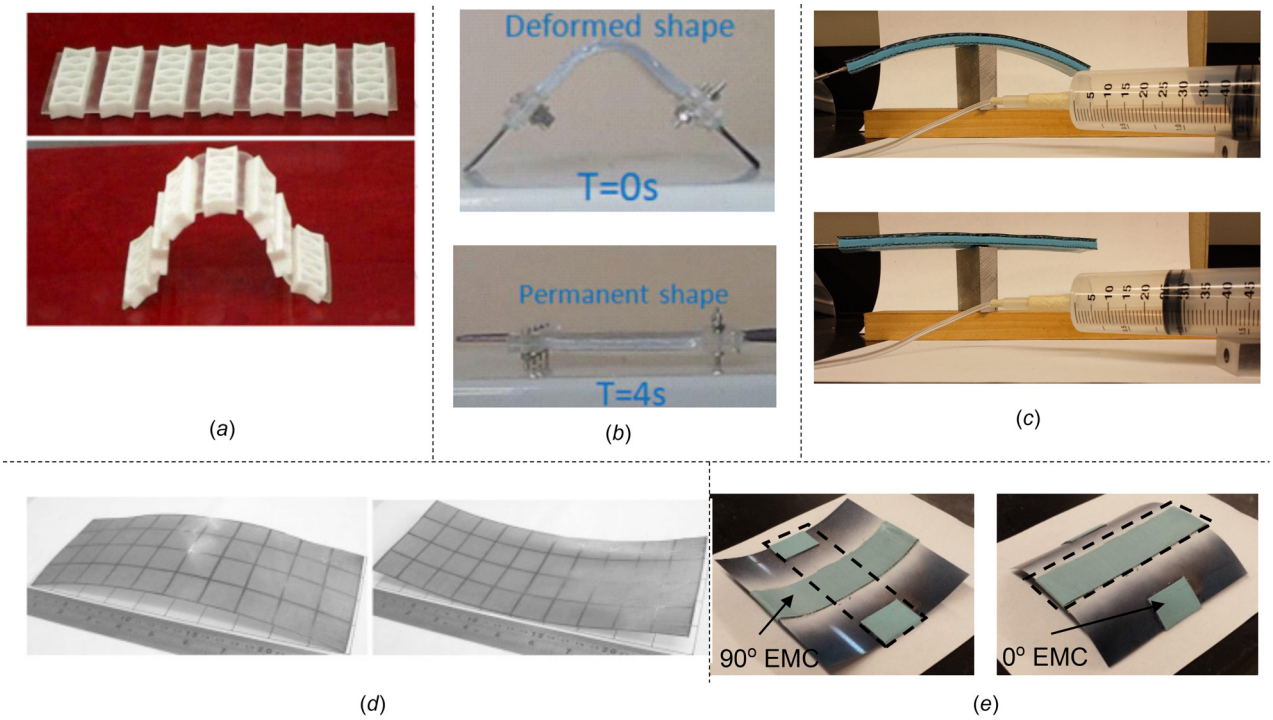

Fig. 7 (*a*) SMPs reinforced with zero-Poisson's ratio honeycombs (reproduced with permission from Huang et al. [110]. Copyright 2017 by Elsevier Ltd.), (*b*) elastomer reinforced with SMA wires that are fused to the matrix (reproduced with permission from Feng et al. [107]. Copyright 2015 by Elsevier Ltd.), (*c*) curved composites with intrinsic pressure actuation and prestress [70], (*d*) bistable buckled laminates with symmetric curved shapes (reproduced with permission from Daynes et al. [117]. Copyright 2008 by Elsevier Ltd.), and (*e*) mechanically prestressed bistable laminates with weakly coupled curved shapes [124].

Table 3 Summary of foldable laminated composites

Feature	Actuator/active element	Analyzed feature	Actuation energy density[a] (kJ/m^3)	Crease stiffness[a]	Advantages (■) and limitations (□)
Lamina emergent torsional joints [131]	External force	Crease	N/A	14,395 N mm/rad	■ Kinematic locking for high stiffness ■ High tensile or compressive stiffness □ Limited flexibility for folding
Mechanically prestressed folds [132,133]	External force	Crease	1.875	N/A	■ Folded initial shape without actuation ■ Prestress enables one-way actuation □ Actuation is required to hold deployed shape
Multistable origami composites [134–136]	External force, pressurized fluid	Folded structure	18	19,100 N mm/rad	■ Rapid switching between folded shapes □ Not realizable when fold faces are rigid
Fluid layer sandwiched between origami sheets [78]	Pressurized fluid	1D tensile origami structure	5300 (open chamber), 18,580 (trapped fluid)	0.91 N/mm (open), 3.19 N/mm (trapped)	■ Controllable shape and stiffness ■ Compatible with nastic actuation
Pressurized elastomeric folded structures [137]	Pressurized air	1D contracting origami structure	375	N/A	■ The foldable structures are also conformable □ High actuation power may be required when used with rigid materials
SMP-activated origami folds [138–140]	Resistive heating of SMPs	Crease	N/A	8.2 N mm/rad	■ Shapes can be fixed and recovered □ Slow thermomechanical response
SMA activated origami folds [141–143]	Torsional SMA wire actuator	Hinge with an embedded SMA	3750	0.143 N mm/rad	■ Attractive for localized actuation □ Low global stiffness of the structure
Electro- and magneto-active folds [144–146]	Electric or magnetic field	Four-layer terpolymer crease	8.7	8.1 N mm/rad	■ Composites respond to multiple fields □ Limited scalability in size

[a]Calculated using the reported values of folding torque, folding range, or actuation energy.

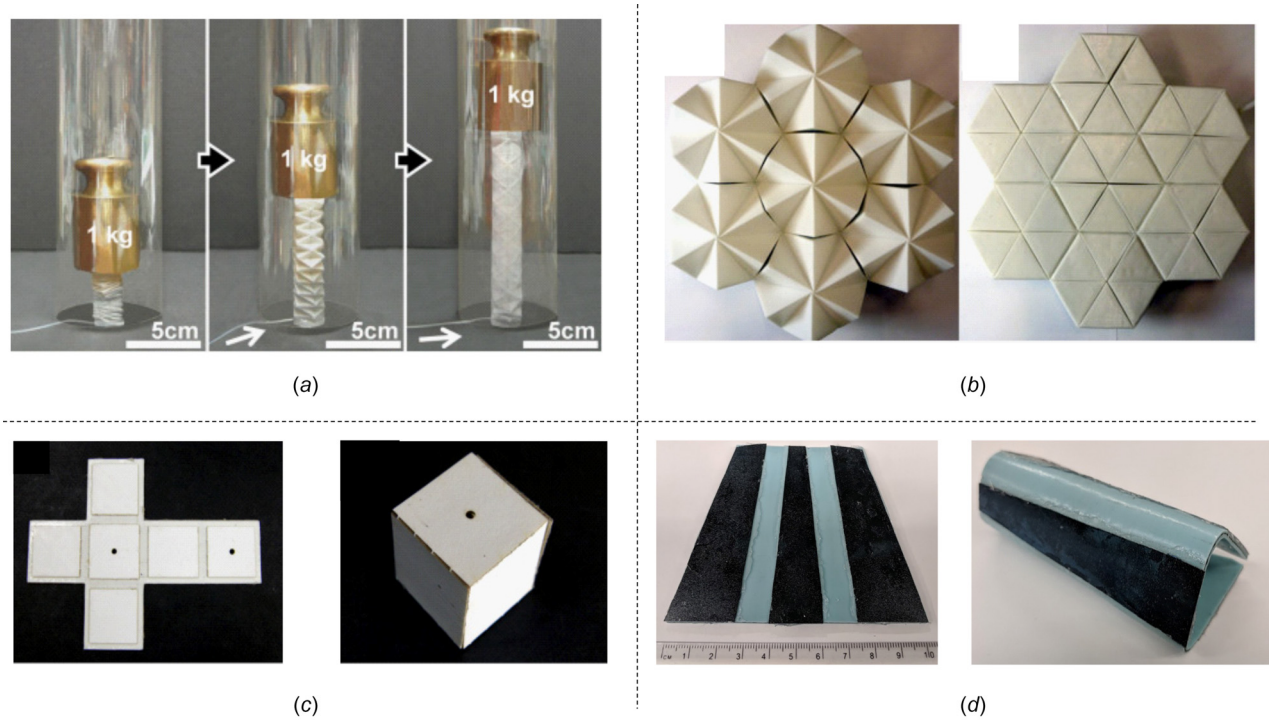

Fig. 8 (*a*) Inflatable paper-elastomer origami composites (reproduced with permission from [137]. Copyright 2017 by Wiley), (*b*) elastomer-acrylonitrile butadiene styrene composites with multistable origami shapes (reproduced with permission from Ref. [134]. Copyright 2017 by IOP Publishing), (*c*) folds created through selective activation of a SMP layer (reproduced with permission from Ref. [140]. Copyright 2017 by IOP Publishing), and (*d*) stress-biased composites with folded stable shapes [133].

Table 4 Strain models for various morphing mechanics

Mechanics	Example cases	Assumptions	Displacements	References
Stretching	Anisotropic skins	$\frac{\partial w}{\partial x}=0,\ \frac{\partial w}{\partial y}=0$	$u(x,y,z)=u_0(x),\ v(x,y,z)=v_0(y)$	[148]
	Zero Poisson's ratio skins	$\frac{\partial w}{\partial x}=0,\ \frac{\partial w}{\partial y}=0,\ \left(\frac{\partial v}{\partial x}\right)^2=0,\ \left(\frac{\partial v}{\partial y}\right)^2=0,\ \left(\frac{\partial u}{\partial y}\right)^2=0$	$u(x,y,z)=u_0(x),\ v(x,y,z)=v_0(y)$	[67]
Flexure	Curved composites, bistable curvatures	$\left(\frac{\partial u}{\partial x}\right)^2=0,\ \left(\frac{\partial v}{\partial x}\right)^2=0,\ \left(\frac{\partial u}{\partial y}\right)^2=0,\ \left(\frac{\partial v}{\partial y}\right)^2=0,\ \frac{\partial u}{\partial x}\frac{\partial u}{\partial y}=0,\ \frac{\partial v}{\partial x}\frac{\partial v}{\partial y}=0$	$u(x,y,z)=u_0(x)-z\frac{\partial w_0}{\partial x},\ v(x,y,z)=v_0(y)-z\frac{\partial w_0}{\partial y},\ w(x,y,z)=w_0(x,y)$	[73, 149, 74, 150]
Folding	Smooth, curved folds	$\left(\frac{\partial u}{\partial x}\right)^2=0,\ \left(\frac{\partial v}{\partial x}\right)^2=0,\ \left(\frac{\partial u}{\partial y}\right)^2=0,\ \left(\frac{\partial v}{\partial y}\right)^2=0,\ \frac{\partial u}{\partial x}\frac{\partial u}{\partial y}=0,\ \frac{\partial v}{\partial x}\frac{\partial v}{\partial y}=0$	$u(x,y,z)=u_0(x)-z\frac{\partial w_0}{\partial x},\ v(x,y,z)=v_0(y)-z\frac{\partial w_0}{\partial y},\ w(x,y,z)=w_0(x,y)$	[151, 133]

shear strain are considered to be minimal. The model is meant for thin to moderately thick composites with geometric nonlinearities. Strains are described using nonlinear expressions based on the Lagrangian formulation and von Karman's hypothesis is used to account for moderate rotations. The deformed shapes are calculated as a function of actuation and external forces using strain energy minimization. Under suitable kinematic assumptions (see Table 4), the model is applicable to stretchable, flexible, or foldable composites. The developments in the modeling of composites for various morphing modes is presented in Sec. 4.2.

4.1 General Analytical Laminated-Plate Model

4.1.1 Laminate Strain Formulation. Reddy [152] showed that strains of an arbitrary point (x, y) on the composite are written in accordance with von Karman's hypothesis as

$$\epsilon_x = \frac{\partial u}{\partial x} + \frac{1}{2}\left[\left(\frac{\partial u}{\partial x}\right)^2 + \left(\frac{\partial v}{\partial x}\right)^2 + \left(\frac{\partial w}{\partial x}\right)^2\right] \quad (1)$$

$$\gamma_{xy} = \frac{\partial u}{\partial y} + \frac{\partial v}{\partial x} + \left[\frac{\partial u}{\partial x}\frac{\partial u}{\partial y} + \frac{\partial v}{\partial x}\frac{\partial v}{\partial y} + \frac{\partial w}{\partial x}\frac{\partial w}{\partial y}\right] \quad (2)$$

$$\epsilon_y = \frac{\partial v}{\partial y} + \frac{1}{2}\left[\left(\frac{\partial u}{\partial y}\right)^2 + \left(\frac{\partial v}{\partial y}\right)^2 + \left(\frac{\partial w}{\partial y}\right)^2\right] \quad (3)$$

The simplified strain expressions for each morphing mode are obtained using the assumptions listed in Table 4. Displacements u, v, and w of an arbitrary point in the composite are related to the geometric midplane's displacements u_0, v_0, and w_0 in the X, Y, and Z directions, respectively, as shown in Table 4. Strains of an arbitrary plane z are obtained by substituting the displacements u, v, w into Eqs. (1)–(3), leading to the relations

$$\epsilon_x = \epsilon_x^0 + z\kappa_x^0, \quad \gamma_{xy} = \gamma_{xy}^0 + z\kappa_{xy}^0, \quad \epsilon_y = \epsilon_y^0 + z\kappa_y^0 \quad (4)$$

where ϵ_x^0 and ϵ_y^0 are the in-plane axial strains, γ_{xy}^0 is the in-plane shear strain, and κ_x^0, κ_y^0, and κ_{xy}^0 are the curvatures and twist, respectively, of the geometric midplane. The κ terms would be zero in the case of stretching.

4.1.2 Strain Energy Computation. The elastic potential energy components can be simplified based on the assumptions of plane stress and strain. The strain energy (U_T) of the composite can be expressed as a function of the geometric and material properties of the laminae as

$$U_T = \int_V \left(\frac{1}{2}\bar{Q}_{11}\epsilon_x^2 + \bar{Q}_{12}\epsilon_x\epsilon_y + \frac{1}{2}\bar{Q}_{22}\epsilon_y^2 + \bar{Q}_{16}\gamma_{xy}\epsilon_x + \bar{Q}_{26}\gamma_{xy}\epsilon_y + \frac{1}{2}\bar{Q}_{66}\gamma_{xy}^2\right) dV \quad (5)$$

where $\{\bar{Q}_{ij}\{i,j = 1,2,6\}\}$ are the plane-stress-reduced stiffness parameters [152].

Residual stress generated through thermal or mechanical sources influences a composite's strain energy. Therefore, the energy term U_T should reflect the contribution of these sources. Thermal strain can be modeled by substituting the strains ϵ_x, ϵ_y, and γ_{xy} with $\epsilon_x - \alpha_x\Delta T$, $\epsilon_y - \alpha_y\Delta T$, and $\gamma_{xy} - \alpha_{xy}\Delta T$, respectively; α_x, α_y, α_{xy} are the coefficients of thermal expansion and ΔT is the difference between the curing and operating temperatures. The ΔT^2 terms are ignored in the calculation. Modeling of thermal strains is typical in the calculation of the stable shapes of thermally cured bistable FRP composites [73].

Residual stress created using mechanically prestressed laminae can be modeled using strain components (e.g., ϵ_x) that are expressed as the difference between the prestrain (ϵ_p) applied prior to lamination and the composite's strain (e.g., $\epsilon_x - \epsilon_p$). This approximation is valid only if the applied prestrain is within the limits of the layer's linear material response. In highly stretchable laminae such as elastomers, the material response is nonlinear and the experimentally measured strain corresponds to a nonlinear expression. Material nonlinearity can be included by expressing the strain energy as the area under the stress–strain curve with $\epsilon_x - \epsilon_p$ as the independent variable.

4.1.3 Work Done on the Composite. The work done by forces and moments generated by actuators and operational loads can be calculated in the variational form. Actuation forces have been modeled in various configurations such as transverse, axial, and embedded, to study the composite deformations [126,153]. In composites where the actuators are integral to the structure, such as fluid-filled chambers, variational work can be expressed directly as a function of composite strains and fluid pressure. In case of a rectangular fluid channel, volumetric change can be expressed as $(1+\epsilon_x)(1+\epsilon_y) - 1$, assuming constant thickness under inflation [70].

The equilibrium shapes of the laminate are obtained by minimizing the net energy using a variational approach. To this end, the strains and out-of-plane displacement are calculated by simultaneously solving a set of n nonlinear equations, corresponding to n unknown displacement coefficients. In the absence of any explicit boundary conditions, the Newton–Raphson approach can be employed to numerically approximate the equilibrium shapes of the laminate. To obtain solutions corresponding to the stable shapes, a constraint on the Jacobian of the system of equations is included in the model. The Jacobian matrix is computed with respect to c_i and is required to be positive definite in order to have a stable solution. In cases where elastic or rigid boundary conditions must be satisfied, a constrained optimization solver such as *fmincon* in MATLAB can be used to solve the equations.

4.2 Modeling of Specific Deformation Modes

4.2.1 Stretchable Composites. The in-plane response of highly stretchable composites, such as EMC, was modeled by Peel and Jensen [148]. The strain of an EMC measured in a uniaxial tensile test (Fig. 9(*a*)) corresponds to a nonlinear strain expression

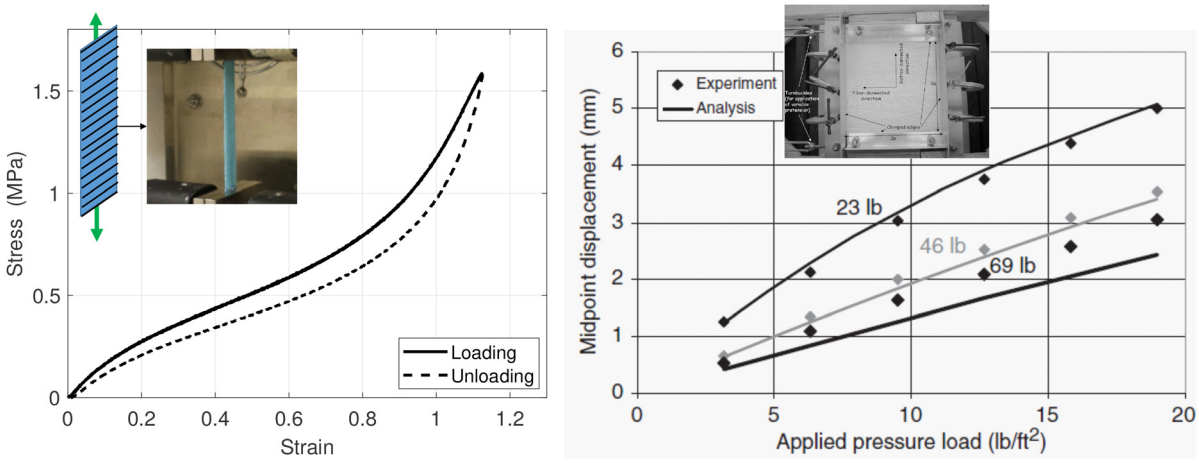

(*a*) (*b*)

Fig. 9 (*a*) Measured stress–strain curve of an EMC with zero in-plane Poisson's ratio. (*b*) Analytical modeling of the out-of-plane stiffness of a flexible matrix composite (reproduced with permission from Murray et al. [67]. Copyright 2010 by SAGE Publications).

of the form $e_x = (\partial u/\partial x) + 0.5(\partial u/\partial x)^2$. For compatibility with classical laminate theory, the nonlinear strain expression was written in linear form. Stress is calculated incrementally at discrete values of linear strain using an experimentally obtained pointwise modulus and described in terms of Ogden coefficients [154].

Modeling of the out-of-plane deformation of stretchable composites is critical in developing skins with high transverse stiffness. Murray et al. [67] used a trigonometric shape function of the form $A\sin(\pi x/a)\cos(\pi y/2b)$ to model the deflection of a rectangular membrane constrained at edges $x = \{-a, a\}$ and $y = \{-b, b\}$ (Fig. 9(*b*)). Murugan et al. [80] developed finite element based multi-objective optimization models to calculate optimal fiber distributions such that the composites require minimal actuation force and have maximum out-of-plane stiffness. Advanced optimization models have been developed based on genetic algorithms to include system parameters such as the number of ribs supporting a stretchable membrane [79].

Laminae with geometric features such as cells and corrugations have been developed as structural reinforcements for stretchable skins. Olympio et al. [81,84] showed that cellular cores have superior strain and stiffness capabilities compared to their constituent materials. In-plane deformation of cellular structures was modeled based on the cellular material theory developed by Gibson and Ashby [155]; the theory describes cell mechanics in terms of small axial and shear deformations of a beam element in a unit cell. Transverse shear deformations were included in the modeling of flexure in these porous cellular cores [81,83]. Cellular structures are strain-limited since their in-plane stiffness increases with increase in in-plane strain. Bai et al. [87] modeled stretchable laminated corrugated panels as thin inextensible curved beams; stiffness of these panels increases as the corrugations flatten and reaches a maximum in the flat state. For corrugations made using FRP composites, the stiffness matrix obtained from laminate theory has been combined with energy expressions to calculate deformations using Castigliano's theorem [88].

The modeling of adaptive stretchable composites is specific to the type and configuration of the active or smart material. As an example, Philen's group [77,156] modeled fluidic actuators for stretching as two cylindrical laminae where the inner elastomeric lamina is isotropic and the outer fiber-reinforced lamina is homogeneous and orthotropic. Smart material-based stretchable-composite modeling includes the homogenized constitutive model for an SMA-reinforced SMP by Song et al. [95].

4.2.2 Flexible Composites. The shapes of flexible composite plates with constant curvature can be calculated by considering the in-plane displacements $u_0(x, y)$ and $v_0(x, y)$ of the geometric midplane to be cubic polynomials and the out-of-plane deflection $w_0(x, y)$ to be a quadratic polynomial containing terms with even power [73,74]. Modeling of bistable composites has received special attention given the design possibilities based on the nonlinear snap-through phenomenon. Beginning with Hyer's analytical model [73], there have been several studies by their group on bistability in thermally cured asymmetric FRP laminates through analytical modeling [74,149,157] and finite element methods [158]. Established on the energy minimization-based analytical modeling, there have been several new designs and configurations of bistable composites [115,159–161] including: symmetric laminates [116], buckled laminates [117], sandwiched metallic cores [71]; and initially curved thermally loaded composites [119]. Chillara and Dapino's model [124] of mechanically prestressed bistable composites includes material and geometric nonlinearities associated with large strain in the prestressed elastomeric layers.

Constant curvature is often assumed in the design of actuation systems for curved composites. Bistable composites actuated by piezoelectric MFC are modeled by including the MFC's stiffness in the potential energy term and voltage input in the form of work done on the composite [123,162]. SMAs have been modeled as embedded actuators because their strain capability of 6% is in the same range as the in-plane strains produced in curved composites. Commonly modeled as wires, these actuators contract upon heating, thereby creating flexure. The SMA returns to its original length when deactivated due to the internal stress in the bent composite. Dano and Hyer [153] modeled SMAs in a tendon configuration. Composite shape was calculated as a function of the forces applied by the wire at its ends. The forces are input as stress, into the SMA's constitutive equation (Brinson model [163]) to calculate actuation temperature. Analytical energy-minimization models and finite element models have been presented for SMA-actuated bistable composites [105,118].

Quadratic approximations of displacement polynomials and the assumption of constant-curvature are accurate for the calculation of stable shapes but not for modeling transitional phenomena such as snap-through loads [164] and the limits of bistability [165,166]. Cantera et al. [167] relaxed the assumptions by considering nonuniform curvature and a uniform through-thickness normal strain. Through a model-order study, Pirrera et al. [168] showed that increasing the polynomial order of the displacement functions results in improved accuracy in the calculation of bifurcation points (Fig. 10(*a*)) and snap-through loads. Beyond seventh-order, the improvement in accuracy is marginal when compared to the increase in computational cost. For asymmetric rectangular laminates with cylindrical stable shapes, the following assumptions were made to simplify the complete displacement polynomials: the composite is clamped at the center; u_0 is odd in x and even in y; v_0 is even in x and odd in y; and w_0 is even in x and y and is zero at the center. The displacements are nondimensionalized to eliminate inaccuracies related to numerical conditioning. Using

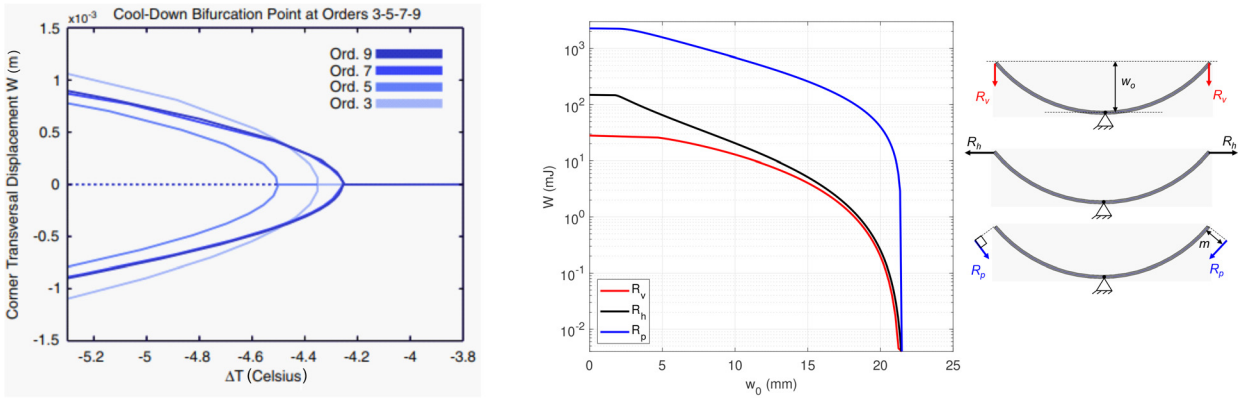

(*a*) (*b*)

Fig. 10 (*a*) Model-order study of shape bifurcation in thermally cured bistable FRP laminates (reproduced with permission from Pirrera et al. [168]. Copyright 2010 by Elsevier Ltd.), (*b*) actuation work (*W*) requirements for the snap-through of bistable composites or the flattening of curved prestressed composites; calculations are performed for mechanically prestressed laminates with dimensions 152.4 × 152.4 × 0.127 mm (see Ref. [125] for details).

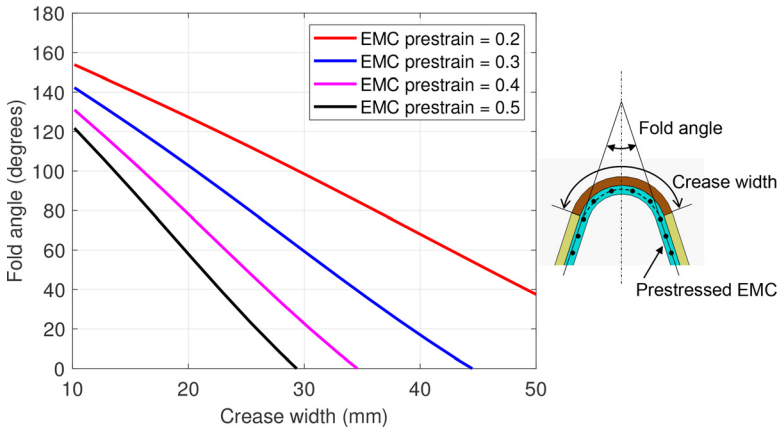

Fig. 11 Fold angle as a function of crease width and EMC prestrain in a stress-biased composite [133]

seventh-order polynomials, a study of actuation-force cases shows that the energy required for embedded actuation is an order of magnitude higher than in the case of an external axial force (Fig. 10(*b*)). However, smart materials can deliver sufficient force and stroke to make embedded actuation a practical approach for curved composites.

4.2.3 Foldable Composites. Folds in laminated composites have been modeled under the assumption of zero in-plane strain and constant global curvature at the crease [151]. Individual creases are modeled under the assumption that the faces are rigid and flat. Fold angle is then calculated using strain energy minimization as a function of material, geometric, and actuation parameters. The assumption of zero in-plane strain is valid only for relatively stiff materials and thin creases. For generic creased composites, however, the modeling should reflect the sharp localized deformations described by folds. Mattioni et al. [150] developed a piecewise-continuous displacement model to calculate localized deformations in composites in the presence of elastic boundary conditions. Using a similar approach, Chillara and Dapino [133] modeled creased composites that have a folded shape due to mechanical prestrain applied to specific laminae in a nonparallel orientation across a crease. Figure 11 shows the relation between fold angle and crease width for the case with prestrain orthogonal to the crease line. To include the effects of the elastic boundary conditions formed by the adjoining faces, the crease is assumed to have nonuniform curvature described by a biquadratic out-of-plane displacement polynomial. While the assumption of constant crease curvature is sufficient to model a fold due to orthogonal prestrain, higher-order polynomials are required to model folds due to nonorthogonal prestrain.

Micromechanics studies of folded reinforced composites have shown that fibers break under large flexure in a stiff matrix such as epoxy [169]. In a soft matrix, however, the fibers buckle without breaking due to the low shear stress [170,171]; the fiber layers that are under compressive stress undergo microbuckling. Francis et al. [172] reviewed analytical models for the microbuckling of the fibers in the soft matrix composites and presented an expression for the wavelength of the buckled fibers. López Jimenez and Pellegrino [171] presented a finite element model of folded fibers in a hyperelastic matrix. Results showed that the fibers undergo in-plane buckling, out-of-plane deformations, and exhibit uniform curvature in the folded region.

The development of origami-folded composites is typically based on experiments and FE analysis of a unit cell of a periodic structure. Parametric studies have been presented to guide the design of various functions such as bistability [136], intrinsic actuation [78,137–139], and 2D–3D transitions through lamina-emergent mechanisms [131].

5 Summary and Outlook

This review highlights the emergence of laminated composites as an attractive design platform for morphing structures. For structural applications, the properties of polymer-based laminated composites have been enhanced through fiber-reinforcements and inclusions in various configurations to provide high stiffness and high strength-to-weight ratio. In the past few decades, this design approach has been employed toward the development of composites that can undergo large deformations and thereby serve as morphing elements. By tailoring the anisotropic material properties of the composite, various morphing modes such as stretching, flexure, twisting, coiling, and folding can be achieved. Further, smart or active layers can be integrated into composite structures to achieve shape and stiffness control (actuation). Emerging applications for these structures in the aerospace, automotive, and robotics industries provide a wide range of opportunities for innovation in design, scalability, lightweighting, safety, and performance. The trade-off with morphing composites is that they should be sufficiently stiff to withstand operational loads, but should provide maximal deformation while consuming minimal actuation energy.

Several new approaches have been presented for tailoring the stiffness of passive materials to achieve large deformations. Smart materials such as piezoelectrics and shape memory alloys and active features such as fluid-filled cavities have been commonly used as shape control elements because of the potential for embedding them or including them as laminae. In this review, a general design framework is presented for composite structures based on three types of laminae, viz., constraining, adaptive, and prestressed (stress-biased). Based on the contributions of several researchers, an analytical modeling framework is also presented as a basis for the design of morphing laminated composites. Given the variety in the available designs, it is challenging to perfectly generalize the modeling approach since the finer modeling details are a function of the choice of laminae (cellular, corrugated, etc.) and laminate configuration.

Analytical modeling of morphing laminates has been predominantly in the direct form where the deformations and shapes are calculated from a known set of material and geometric properties. However, there is a need for analytical tools based on an inverse approach that guide the selection and design of materials and laminate structure based on a set of known deformed shapes. This type of modeling would entail the use of optimization tools, neural networks, etc., under a given set of material constraints. A deeper understanding of composite scalability is also needed because there are several opportunities for the design of nonlinear characteristics based on material and geometric nonlinearities. For example, the nonlinear response of bistable or buckled composites

is a function of their shape and size and can be tailored to minimize the energy required to actuate the structure. Modeling of adaptive laminae often involves multiple physics such as structural mechanics, fluid–structure interaction, and heat transfer. In this scenario, finite element analysis is more efficient relative to analytical modeling. This review does not discuss finite element analysis efforts in detail due to the great variety in designs and design-specific models in the literature.

Despite a wide range of designs on multifunctional composites, the field of morphing structures is still emerging. In the field of morphing aircraft, there have been significant advancements in morphing unmanned aerial vehicles and a few technologies have matured into applications on commercial aircraft. In the automotive industry, recent concept-vehicles have featured morphing panels, but the research is in the early stages. Compliant-robotics applications have evolved rapidly and there are promising concepts based on multifunctional composites. The challenges common to all fields are design scalability, repeatability of morphing response, durability (e.g., viscoelastic effects such as creep in compliant materials), and tolerance to extreme conditions. In this scenario, multifunctional laminated composites are promising because of the possibility for creating hybrid structures with special geometric and material properties to address the various challenges that lay in the path of realizing morphing structures in real-world applications.

Acknowledgment

Financial support was provided by the member organizations of the Smart Vehicle Concepts Center,[2] a Phase III National Science Foundation Industry-University Cooperative Research Center under grant NSF IIP 1738723.

Nomenclature

CFRP = carbon fiber-reinforced polymer
EMC = elastomeric matrix composite
FE = finite element
FRP = fiber-reinforced polymer
MFC = macrofiber composite
$\bar{Q}_{ij}$ = reduced transformed stiffness coefficients
SMA = shape memory alloy
SMP = shape memory polymer
T_g = glass transition temperature
u, v, w = displacements in the X, Y, Z directions, respectively
u_0, v_0, w_0 = displacements of the midplane
U_T = strain energy of the composite
x, y, z = coordinates
X, Y, Z = coordinate axes
$\alpha_x, \alpha_y, \alpha_{xy}$ = coefficients of thermal expansion
ΔT = change in temperature
ϵ_p = prestrain applied to a lamina
$\epsilon_x, \epsilon_y, \epsilon_{xy}$ = von Karman strains
$\epsilon_x^0, \epsilon_y^0, \epsilon_{xy}^0$ = strains of the midplane
$\kappa_x^0, \kappa_y^0, \kappa_{xy}^0$ = curvatures of the midplane

References

[1] Lentink, D., Müller, U. K., Stamhuis, E. J., de Kat, R., van Gestel, W., Veldhuis, L. L. M., Henningsson, P., Hedenström, A., Videler, J. J., and van Leeuwen, J. L., 2007, "How Swifts Control Their Glide Performance With Morphing Wings," Nature, **446**(7139), pp. 1082–1085.
[2] Forterre, Y., Skotheim, J. M., Dumais, J., and Mahadevan, L., 2005, "How the Venus Flytrap Snaps," Nature, **433**(7024), pp. 421–425.
[3] Barbarino, S., Bilgen, O., Ajaj, R. M., Friswell, M. I., and Inman, D. J., 2011, "A Review of Morphing Aircraft," J. Intell. Mater. Syst. Struct., **22**(9), pp. 823–877.
[4] McGowan, A.-M. R., Horta, L. G., Harrison, J. S., and Raney, D. L., 2000, "Research Activities Within NASA's Morphing Program," National Aeronautics and Space Administration, Langley Research Center, Hampton, VA, Accession No. ADP010487.
[5] Daynes, S., and Weaver, P. M., 2013, "Review of Shape-Morphing Automobile Structures: Concepts and Outlook," Proc. Inst. Mech. Eng., Part D, **227**(11), pp. 1603–1622.
[6] Chu, W.-S., Lee, K.-T., Song, S.-H., Han, M.-W., Lee, J.-Y., Kim, H.-S., Kim, M.-S., Park, Y.-J., Cho, K.-J., and Ahn, S.-H., 2012, "Review of Biomimetic Underwater Robots Using Smart Actuators," Int. J. Precis. Eng. Manuf., **13**(7), pp. 1281–1292.
[7] Laschi, C., Mazzolai, B., and Cianchetti, M., 2016, "Soft Robotics: Technologies and Systems Pushing the Boundaries of Robot Abilities," Sci. Rob., **1**(1), eaah3690.
[8] Apuleo, G., 2018, "Chapter 2—Aircraft Morphing: An Industry Vision," *Morphing Wing Technologies*, Elsevier, Oxford, UK, pp. 85–101.
[9] Bowman, J., Sanders, B., and Weisshaar, T., 2002, "Evaluating the Impact of Morphing Technologies on Aircraft Performance," AIAA Paper No. 2002-1631.
[10] Thill, C., Etches, J., Bond, I., Potter, K., and Weaver, P., 2008, "Morphing Skins," Aeronaut. J., **112**(1129), pp. 117–139.
[11] Sofla, A. Y. N., Meguid, S. A., Tan, K. T., and Yeo, W. K., 2010, "Shape Morphing of Aircraft Wing: Status and Challenges," Mater. Des., **31**(3), pp. 1284–1292.
[12] Weisshaar, T. A., 2013, "Morphing Aircraft Systems: Historical Perspectives and Future Challenges," J. Aircr., **50**(2), pp. 337–353.
[13] Poulin, J.-R., Terriault, P., Dubé, M., and Vachon, P.-L., 2017, "Development of a Morphing Wing Extrados Made of Composite Materials and Actuated by Shape Memory Alloys," J. Intell. Mater. Syst. Struct., **28**(11), pp. 1437–1453.
[14] Han, M.-W., Rodrigue, H., Kim, H.-I., Song, S.-H., and Ahn, S.-H., 2016, "Shape Memory Alloy/Glass Fiber Woven Composite for Soft Morphing Winglets of Unmanned Aerial Vehicles," Compos. Struct., **140**, pp. 202–212.
[15] Dayyani, I., Shaw, A. D., Saavedra Flores, E. I., and Friswell, M. I., 2015, "The Mechanics of Composite Corrugated Structures: A Review With Applications in Morphing Aircraft," Compos. Struct., **133**, pp. 358–380.
[16] Gong, X., Liu, L., Scarpa, F., Leng, J., and Liu, Y., 2017, "Variable Stiffness Corrugated Composite Structure With Shape Memory Polymer for Morphing Skin Applications," Smart Mater. Struct., **26**(3), p. 035052.
[17] Kochersberger, K. B., Ohanian, O. J., Probst, T., and Gelhausen, P. A., 2017, "Design and Flight Test of the Generic Micro-Aerial Vehicle (GenMAV) Utilizing Piezoelectric Conformal Flight Control Actuation," J. Intell. Mater. Syst. Struct., **28**(19), pp. 2793–2809.
[18] Bilgen, O., Kochersberger, K. B., Inman, D. J., and Ohanian, O. J., 2010, "Novel, Bidirectional, Variable-Camber Airfoil Via Macro-Fiber Composite Actuators," J. Aircr., **47**(1), pp. 303–314.
[19] Nicassio, F., Scarselli, G., Pinto, F., Ciampa, F., Iervolino, O., and Meo, M., 2018, "Low Energy Actuation Technique of Bistable Composites for Aircraft Morphing," Aerosp. Sci. Technol., **75**, pp. 35–46.
[20] Lachenal, X., Daynes, S., and Weaver, P. M., 2014, "A Non-Linear Stiffness Composite Twisting i-Beam," J. Intell. Mater. Syst. Struct., **25**(6), pp. 744–754.
[21] Daynes, S., Lachenal, X., and Weaver, P. M., 2015, "Concept for Morphing Airfoil With Zero Torsional Stiffness," Thin-Walled Struct., **94**, pp. 129–134.
[22] Jenett, B., Calisch, S., Cellucci, D., Cramer, N., Gershenfeld, N., Swei, S., and Cheung, K. C., 2017, "Digital Morphing Wing: Active Wing Shaping Concept Using Composite Lattice-Based Cellular Structures," Soft Rob., **4**(1), pp. 33–48.
[23] Rudenko, A., Hannig, A., Monner, H. P., and Horst, P., 2018, "Extremely Deformable Morphing Leading Edge: Optimization, Design and Structural Testing," J. Intell. Mater. Syst. Struct., **29**(5), pp. 764–773.
[24] Vasista, S., Nolte, F., Monner, H. P., Horst, P., and Burnazzi, M., 2018, "Three-Dimensional Design of a Large-Displacement Morphing Wing Droop Nose Device," J. Intell. Mater. Syst. Struct., **29**(16), pp. 3222–3241.
[25] Daynes, S., Weaver, P., and Trevarthen, J., 2011, "A Morphing Composite Air Inlet With Multiple Stable Shapes," J. Intell. Mater. Syst. Struct., **22**(9), pp. 961–973.
[26] Arena, G., Groh, R. M. J., Brinkmeyer, A., Theunissen, R., Weaver, P. M., and Pirrera, A., 2017, "Adaptive Compliant Structures for Flow Regulation," Proc. Math., Phys., Eng. Sci., **473**(2204), p. 20170334.
[27] Sun, J., Guan, Q., Liu, Y., and Leng, J., 2016, "Morphing Aircraft Based on Smart Materials and Structures: A State-of-the-Art Review," J. Intell. Mater. Syst. Struct., **27**(17), pp. 2289–2312.
[28] Systems, H.-D., 2013, "Future US Trends in the Adoption of Light-Duty Automotive Technologies," American Petroleum Institute, Washington, DC, Integrated Final Report.
[29] Ando, K., Kuratani, N., and Fukuda, H., 2016, "Aerodynamic Performance Evaluation System at the Early Concept Stage of Automotive Styling Development Based on CFD," SAE Paper No. 2016-01-1584.
[30] Hucho, W. H., 1987, *Aerodynamics of Road Vehicles: From Fluid Mechanics to Vehicle Engineering*, Butterworth-Heinemann, Oxford, UK.
[31] Barnard, R. H., 1996, *Road Vehicle Aerodynamic Design—An Introduction*, Addison Wesley Longman Limited, Essex, UK.
[32] Koike, M., Nagayoshi, T., and Hamamoto, N., 2004, "Research on Aerodynamic Drag Reduction by Vortex Generators," Mitshubishi Motors Tech. Rev., **16**, pp. 11–16.
[33] Sunny, S. A., 2011, "Effect of Turbulence in Modeling the Reduction of Local Drag Forces in a Computational Automotive Model," Int. J. Energy Environ., **2**(6), pp. 1079–1100.

[2] www.SmartVehicleCenter.org

[34] Hucho, W.-H., and Ahmed, S. R., 1998, *Aerodynamics of Road Vehicles: From Fluid Mechanics to Vehicle Engineering*, Society of Automotive Engineers, Warrendale, PA.
[35] Buchheim, R., Leie, B., and Lückoff, H., 1983, "Der Neue Audi 100–Ein Beispiel Für Konsequente Aerodynamische Personenwagen-Entwicklung," Automobiltechnische Z., **85**, pp. 419–425.
[36] Costelli, A. F., 1984, "Aerodynamic Characteristics of the Fiat UNO Car," SAE Paper No. 840297.
[37] BMW, 2016, "BMW Vision Next 100 Years Concept," Bayerische Motoren Werke Aktiengesellschaft, Mönchen, Germany, accessed July 25, 2019, https://www.bmwgroup.com/en/company/the-next-100-years/brandvisions.html#BMW
[38] Daimler, 2015, "Mercedes-Benz Intelligent Aerodynamic Automobile: Digital Transformer," Mercedes AG, Stuttgart, Germany, accessed July 25, 2019, https://media.daimler.com/marsMediaSite/en/instance/ko/Mercedes-Benz-Concept-IAA-Intelligent-Aerodynamic-Automobile-Digital-transformer.xhtml?oid=9904826
[39] Porsche, 2017, "Porsche Active Aerodynamics (PAA)," Porsche AG, Stuttgart, Germany, accessed July 25, 2019, https://www.porsche.com/international/models/911/911-turbo-models/911-turbo/chassis/porsche-active-aerodynamics-paa/
[40] Ferrari, 2014, "Ferrari 458 Speciale Active Aerodynamics," Ferrari S. p. A., Maranello, Italy, July 25, 2019, https://auto.ferrari.com/en_US/sports-cars-models/past-models/458-speciale/#innovations-aerodynamics-3
[41] Chillara, V. S. C., Headings, L. M., Tsuruta, R., Gandhi, U., Itakura, E., and Dapino, M. J., 2018, "Shape Memory Alloy-Actuated Prestressed Composites With Application to Morphing Automotive Fender Skirts," J. Intell. Mater. Syst. Struct., **30**(3), pp. 479–494.
[42] Han, M.-W., Rodrigue, H., Cho, S., Song, S.-H., Wang, W., Chu, W.-S., and Ahn, S.-H., 2016, "Woven Type Smart Soft Composite for Soft Morphing Car Spoiler," Compos. Part B Eng., **86**, pp. 285–298.
[43] Spiteri, L., Daynes, S., and Watkins, S., 2015, "Design of a Morphing Bi-Stable Composite Air Intake," SAE Paper No. 2015-01-0066.
[44] Qamar, I. P. S., Groh, R., Holman, D., and Roudaut, A., 2018, "HCI Meets Material Science: A Literature Review of Morphing Materials for the Design of Shape-Changing Interfaces," CHI Conference on Human Factors in Computing Systems (CHI), Montreal QC, Canada, Apr. 21–26, Paper No. 374.
[45] Lachenal, X., Daynes, S., and Weaver, P. M., 2013, "Review of Morphing Concepts and Materials for Wind Turbine Blade Applications," Wind Energy, **16**(2), pp. 283–307.
[46] Hayat, K., and Ha, S. K., 2015, "Load Mitigation of Wind Turbine Blade by Aeroelastic Tailoring Via Unbalanced Laminates Composites," Compos. Struct., **128**, pp. 122–133.
[47] Herath, M. T., Lee, A. K. L., and Prusty, B. G., 2015, "Design of Shape-Adaptive Wind Turbine Blades Using Differential Stiffness Bend–Twist Coupling," Ocean Eng., **95**, pp. 157–165.
[48] Arrieta, A. F., Kuder, I. K., Rist, M., Waeber, T., and Ermanni, P., 2014, "Passive Load Alleviation Aerofoil Concept With Variable Stiffness Multi-Stable Composites," Compos. Struct., **116**, pp. 235–242.
[49] Fortini, A., Suman, A., Merlin, M., and Garagnani, G. L., 2015, "Morphing Blades With Embedded SMA Strips: An Experimental Investigation," Mater. Design, **85**, pp. 785–795.
[50] Fortini, A., Suman, A., Aldi, N., Merlin, M., and Pinelli, M., 2015, "A Shape Memory Alloy-Based Morphing Axial Fan Blade—Part 1: Blade Structure Design and Functional Characterization," ASME J. Eng. Gas Turbines Power, **138**(2), p. 022601.
[51] Rus, D., and Tolley, M. T., 2015, "Design, Fabrication and Control of Soft Robots," Nature, **521**(7553), pp. 467–475.
[52] Cao, J., Qin, L., Liu, J., Ren, Q., Foo, C. C., Wang, H., Lee, H. P., and Zhu, J., 2018, "Untethered Soft Robot Capable of Stable Locomotion Using Soft Electrostatic Actuators," Extreme Mech. Lett., **21**, pp. 9–16.
[53] Rus, D., and Tolley, M. T., 2018, "Design, Fabrication and Control of Origami Robots," Nat. Rev. Mater., **3**(6), pp. 101–112.
[54] Manti, M., Cacucciolo, V., and Cianchetti, M., 2016, "Stiffening in Soft Robotics: A Review of the State of the Art," IEEE Rob. Autom. Mag./IEEE Rob. Autom. Soc., **23**(3), pp. 93–106.
[55] Li, S., and Wang, K. W., 2016, "Plant-Inspired Adaptive Structures and Materials for Morphing and Actuation: A Review," Bioinspiration Biomimetics, **12**(1), p. 011001.
[56] Jin, H., Dong, E., Alici, G., Mao, S., Min, X., Liu, C., Low, K. H., and Yang, J., 2016, "A Starfish Robot Based on Soft and Smart Modular Structure (SMS) Actuated by SMA Wires," Bioinspiration Biomimetics, **11**(5), p. 056012.
[57] Yeom, S.-W., and Oh, I.-K., 2009, "A Biomimetic Jellyfish Robot Based on Ionic Polymer Metal Composite Actuators," Smart Mater. Struct., **18**(8), p. 085002.
[58] Wang, W., Lee, J.-Y., Rodrigue, H., Song, S.-H., Chu, W.-S., and Ahn, S.-H., 2014, "Locomotion of Inchworm-Inspired Robot Made of Smart Soft Composite (SSC)," Bioinspiration Biomimetics, **9**(4), p. 046006.
[59] Kim, H.-J., Song, S.-H., and Ahn, S.-H., 2012, "A Turtle-Like Swimming Robot Using a Smart Soft Composite (SSC) Structure," Smart Mater. Struct., **22**(1), p. 014007.
[60] Marchese, A. D., Katzschmann, R. K., and Rus, D., 2015, "A Recipe for Soft Fluidic Elastomer Robots," Soft Rob., **2**(1), pp. 7–25.
[61] Puig, L., Barton, A., and Rando, N., 2010, "A Review on Large Deployable Structures for Astrophysics Missions," Acta Astronaut., **67**(1–2), pp. 12–26.
[62] Lake, M., Munshi, N., Meink, T., and Tupper, M., 2001, "Application of Elastic Memory Composite Materials to Deployable Space Structures," AIAA Paper No. 2001-4602.
[63] Wang, W., Rodrigue, H., and Ahn, S.-H., 2016, "Deployable Soft Composite Structures," Sci. Rep., **6**, p. 20869.
[64] Costantine, J., Tawk, Y., Christodoulou, C. G., Banik, J., and Lane, S., 2012, "CubeSat Deployable Antenna Using Bistable Composite Tape-Springs," IEEE Antennas Wireless Propag. Lett., **11**, pp. 285–288.
[65] Murphey, T., and Pellegrino, S., 2004, "A Novel Actuated Composite Tape-Spring for Deployable Structures," AIAA Paper No. 2004-1528.
[66] Kikuta, M. T., 2003, "Mechanical Properties of Candidate Materials for Morphing Wings," Master's thesis, Virginia Polytechnic Institute and State University, Blacksburg, VA.
[67] Murray, G., Gandhi, F., and Bakis, C., 2010, "Flexible Matrix Composite Skins for One-Dimensional Wing Morphing," J. Intell. Mater. Syst. Struct., **21**(17), pp. 1771–1781.
[68] Bubert, E. A., Woods, B. K. S., Lee, K., Kothera, C. S., and Wereley, N. M., 2010, "Design and Fabrication of a Passive 1D Morphing Aircraft Skin," J. Intell. Mater. Syst. Struct., **21**(17), pp. 1699–1717.
[69] Lachenal, X., Weaver, P. M., and Daynes, S., 2012, "Multi-Stable Composite Twisting Structure for Morphing Applications," Proc. R. Soc. A, **468**(2141), pp. 1230–1251.
[70] Chillara, V. S. C., Headings, L. M., and Dapino, M. J., 2016, "Multifunctional Composites With Intrinsic Pressure Actuation and Prestress for Morphing Structures," Compos. Struct., **157**, pp. 265–274.
[71] Daynes, S., and Weaver, P., 2010, "Analysis of Unsymmetric CFRP–Metal Hybrid Laminates for Use in Adaptive Structures," Compos. Part A, **41**(11), pp. 1712–1718.
[72] Hyer, M. W., 1981, "Some Observations on the Cured Shape of Thin Unsymmetric Laminates," J. Compos. Mater., **15**(2), pp. 175–194.
[73] Hyer, M. W., 1982, "The Room-Temperature Shapes of Four-Layer Unsymmetric Cross-Ply Laminates," J. Compos. Mater., **16**(4), pp. 318–340.
[74] Dano, M.-L., and Hyer, M. W., 1998, "Thermally-Induced Deformation Behavior of Unsymmetric Laminates," Int. J. Solids Struct., **35**(17), pp. 2101–2120.
[75] Huber, J. E., Fleck, N. A., and Ashby, M. F., 1997, "The Selection of Mechanical Actuators Based on Performance Indices," Proc. R. Soc. A, **453**(1965), pp. 2185–2205.
[76] Feng, N., Liu, L., Liu, Y., and Leng, J., 2015, "A Bio-Inspired, Active Morphing Skin for Camber Morphing Structures," Smart Mater. Struct., **24**(3), p. 035023.
[77] Shan, Y., Philen, M., Lotfi, A., Li, S., Bakis, C. E., Rahn, C. D., and Wang, K.-W., 2009, "Variable Stiffness Structures Utilizing Fluidic Flexible Matrix Composites," J. Intell. Mater. Syst. Struct., **20**(4), pp. 443–456.
[78] Li, S., and Wang, K. W., 2015, "Fluidic Origami: A Plant-Inspired Adaptive Structure With Shape Morphing and Stiffness Tuning," Smart Mater. Struct., **24**(10), p. 105031.
[79] Woods, B. K. S., and Friswell, M. I., 2015, "The Adaptive Aspect Ratio Morphing Wing: Design Concept and Low Fidelity Skin Optimization," Aerosp. Sci. Technol., **42**, pp. 209–217.
[80] Murugan, S., Saavedra Flores, E. I., Adhikari, S., and Friswell, M. I., 2012, "Optimal Design of Variable Fiber Spacing Composites for Morphing Aircraft Skins," Compos. Struct., **94**(5), pp. 1626–1633.
[81] Olympio, K. R., and Gandhi, F., 2010, "Zero Poisson's Ratio Cellular Honeycombs for Flex Skins Undergoing One-Dimensional Morphing," J. Intell. Mater. Syst. Struct., **21**(17), pp. 1737–1753.
[82] Murray, G. J., and Gandhi, F., 2013, "Auxetic Honeycombs With Lossy Polymeric Infills for High Damping Structural Materials," J. Intell. Mater. Syst. Struct., **24**(9), pp. 1090–1104.
[83] Gong, X., Huang, J., Scarpa, F., Liu, Y., and Leng, J., 2015, "Zero Poisson's Ratio Cellular Structure for Two-Dimensional Morphing Applications," Compos. Struct., **134**, pp. 384–392.
[84] Olympio, K. R., and Gandhi, F., 2010, "Flexible Skins for Morphing Aircraft Using Cellular Honeycomb Cores," J. Intell. Mater. Syst. Struct., **21**(17), pp. 1719–1735.
[85] Dayyani, I., Ziaei-Rad, S., and Friswell, M. I., 2014, "The Mechanical Behavior of Composite Corrugated Core Coated With Elastomer for Morphing Skins," J. Compos. Mater., **48**(13), pp. 1623–1636.
[86] Previtali, F., Arrieta, A. F., and Ermanni, P., 2015, "Double-Walled Corrugated Structure for Bending-Stiff Anisotropic Morphing Skins," J. Intell. Mater. Syst. Struct., **26**(5), pp. 599–613.
[87] Bai, J. B., Chen, D., Xiong, J. J., and Shenoi, R. A., 2017, "A Corrugated Flexible Composite Skin for Morphing Applications," Compos. Part B Eng., **131**, pp. 134–143.
[88] Ghabezi, P., 2018, "Rectangular and Triangular Corrugated Composite Skins," Fibers Polym., **19**(2), pp. 435–445.
[89] Philen, M., Shan, Y., Bakis, C., Wang, K.-W., and Rahn, C., 2006, "Variable Stiffness Adaptive Structures Utilizing Hydraulically Pressurized Flexible Matrix Composites With Valve Control," AIAA Paper No. 2006-2134.
[90] Chen, Y., Yin, W., Liu, Y., and Leng, J., 2011, "Structural Design and Analysis of Morphing Skin Embedded With Pneumatic Muscle Fibers," Smart Mater. Struct., **20**(8), p. 085033.
[91] Pikul, J. H., Li, S., Bai, H., Hanlon, R. T., Cohen, I., and Shepherd, R. F., 2017, "Stretchable Surfaces With Programmable 3D Texture Morphing for Synthetic Camouflaging Skins," Science, **358**(6360), pp. 210–214.
[92] Yin, W. L., Sun, Q. J., Zhang, B., Liu, J. C., and Leng, J. S., 2008, "Seamless Morphing Wing With SMP Skin," Adv. Mater. Res., **47–50**, pp. 97–100.
[93] Chen, S., Chen, Y., Zhang, Z., Liu, Y., and Leng, J., 2014, "Experiment and Analysis of Morphing Skin Embedded With Shape Memory Polymer Composite Tube," J. Intell. Mater. Syst. Struct., **25**(16), pp. 2052–2059.

[94] Sun, J., Liu, Y., and Leng, J., 2015, "Mechanical Properties of Shape Memory Polymer Composites Enhanced by Elastic Fibers and Their Application in Variable Stiffness Morphing Skins," J. Intell. Mater. Syst. Struct., **26**(15), pp. 2020–2027.
[95] Song, J. J., Chen, Q., and Naguib, H. E., 2016, "Constitutive Modeling and Experimental Validation of the Thermo-Mechanical Response of a Shape Memory Composite Containing Shape Memory Alloy Fibers and Shape Memory Polymer Matrix," J. Intell. Mater. Syst. Struct., **27**(5), pp. 625–641.
[96] Leng, J., Lan, X., Liu, Y., and Du, S., 2011, "Shape-Memory Polymers and Their Composites: Stimulus Methods and Applications," Prog. Mater. Sci., **56**(7), pp. 1077–1135.
[97] Yokozeki, T., Takeda, S.-I., Ogasawara, T., and Ishikawa, T., 2006, "Mechanical Properties of Corrugated Composites for Candidate Materials of Flexible Wing Structures," Compos. Part A, **37**(10), pp. 1578–1586.
[98] Dayyani, I., Khodaparast, H. H., Woods, B. K. S., and Friswell, M. I., 2015, "The Design of a Coated Composite Corrugated Skin for the Camber Morphing Airfoil," J. Intell. Mater. Syst. Struct., **26**(13), pp. 1592–1608.
[99] Deimel, R., and Brock, O., 2013, "A Compliant Hand Based on a Novel Pneumatic Actuator," IEEE International Conference on Robotics and Automation (ICRA), Karlsruhe, Germany, May 6–10, pp. 2047–2053.
[100] Marchese, A. D., Onal, C. D., and Rus, D., 2014, "Autonomous Soft Robotic Fish Capable of Escape Maneuvers Using Fluidic Elastomer Actuators," Soft Rob., **1**(1), pp. 75–87.
[101] Yao, L., Niiyama, R., Ou, J., Follmer, S., Della Silva, C., and Ishii, H., 2013, "PneUI: Pneumatically Actuated Soft Composite Materials for Shape Changing Interfaces," 26th Annual ACM Symposium on User Interface Software and Technology, Scotland, UK, Oct. 8–11, pp. 13–22.
[102] Pagitz, M., Lamacchia, E., and Hol, J. M. A. M., 2012, "Pressure-Actuated Cellular Structures," Bioinspiration Biomimetics, **7**(1), p. 016007.
[103] Pagitz, M., and Bold, J., 2013, "Shape-Changing Shell-Like Structures," Bioinspiration Biomimetics, **8**(1), p. 016010.
[104] Villanueva, A. A., Joshi, K. B., Blottman, J. B., and Priya, S., 2010, "A Bio-Inspired Shape Memory Alloy Composite (BISMAC) Actuator," Smart Mater. Struct., **19**(2), p. 025013.
[105] Lacasse, S., Terriault, P., Simoneau, C., and Brailovski, V., 2015, "Design, Manufacturing, and Testing of an Adaptive Composite Panel With Embedded Shape Memory Alloy Actuators," J. Intell. Mater. Syst. Struct., **26**(15), pp. 2055–2072.
[106] Rodrigue, H., Bhandari, B., Han, M.-W., and Ahn, S.-H., 2015, "A Shape Memory Alloy–Based Soft Morphing Actuator Capable of Pure Twisting Motion," J. Intell. Mater. Syst. Struct., **26**(9), pp. 1071–1078.
[107] Feng, N., Liu, L., Liu, Y., and Leng, J., 2015, "Characteristics of Multi-Functional Composites Using Elastomer Embedded With Shape Memory Alloy Wires," Mater. Des., **88**, pp. 75–81.
[108] Wang, W., Rodrigue, H., and Ahn, S.-H., 2015, "Smart Soft Composite Actuator With Shape Retention Capability Using Embedded Fusible Alloy Structures," Compos. Part B Eng., **78**, pp. 507–514.
[109] Lelieveld, C., Jansen, K., and Teuffel, P., 2016, "Mechanical Characterization of a Shape Morphing Smart Composite With Embedded Shape Memory Alloys in a Shape Memory Polymer Matrix," J. Intell. Mater. Syst. Struct., **27**(15), pp. 2038–2048.
[110] Huang, J., Zhang, Q., Scarpa, F., Liu, Y., and Leng, J., 2017, "Shape Memory Polymer-Based Hybrid Honeycomb Structures With Zero Poisson's Ratio and Variable Stiffness," Compos. Struct., **179**, pp. 437–443.
[111] Zhang, C.-S., and Ni, Q.-Q., 2007, "Bending Behavior of Shape Memory Polymer Based Laminates," Compos. Struct., **78**(2), pp. 153–161.
[112] Takeda, T., Shindo, Y., and Narita, F., 2015, "Flexural Stiffness Variations of Woven Carbon Fiber Composite/Shape Memory Polymer Hybrid Layered Beams," J. Compos. Mater., **49**(2), pp. 209–216.
[113] Maples, H. A., Wakefield, S., Robinson, P., and Bismarck, A., 2014, "High Performance Carbon Fibre Reinforced Epoxy Composites With Controllable Stiffness," Compos. Sci. Technol., **105**, pp. 134–143.
[114] Robinson, P., Bismarck, A., Zhang, B., and Maples, H. A., 2017, "Deployable, Shape Memory Carbon Fibre Composites Without Shape Memory Constituents," Compos. Sci. Technol., **145**, pp. 96–104.
[115] Li, H., Dai, F., Weaver, P. M., and Du, S., 2014, "Bistable Hybrid Symmetric Laminates," Compos. Struct., **116**, pp. 782–792.
[116] Daynes, S., Diaconu, C. G., Potter, K. D., and Weaver, P. M., 2010, "Bistable Prestressed Symmetric Laminates," J. Compos. Mater., **44**(9), pp. 1119–1137.
[117] Daynes, S., Potter, K. D., and Weaver, P. M., 2008, "Bistable Prestressed Buckled Laminates," Compos. Sci. Technol., **68**(15–16), pp. 3431–3437.
[118] Hufenbach, W., Gude, M., and Czulak, A., 2006, "Actor-Initiated Snap-Through of Unsymmetric Composites With Multiple Deformation States," J. Mater. Process. Technol., **175**(1–3), pp. 225–230.
[119] Eckstein, E., Pirrera, A., and Weaver, P. M., 2014, "Multi-Mode Morphing Using Initially Curved Composite Plates," Compos. Struct., **109**, pp. 240–245.
[120] Schultz, M. R., Hyer, M. W., Brett Williams, R., Keats Wilkie, W., and Inman, D. J., 2006, "Snap-Through of Unsymmetric Laminates Using Piezocomposite Actuators," Compos. Sci. Technol., **66**(14), pp. 2442–2448.
[121] Kim, H. A., Betts, D. N., Salo, A. I. T., and Bowen, C. R., 2010, "Shape Memory Alloy-Piezoelectric Active Structures for Reversible Actuation of Bistable Composites," Am. Inst. Aeronaut. Astronaut. J., **48**(6), pp. 1265–1268.
[122] Lee, A. J., Moosavian, A., and Inman, D. J., 2017, "A Piezoelectrically Generated Bistable Laminate for Morphing," Mater. Lett., **190**, pp. 123–126.
[123] Gude, M., Hufenbach, W., and Kirvel, C., 2011, "Piezoelectrically Driven Morphing Structures Based on Bistable Unsymmetric Laminates," Compos. Struct., **93**(2), pp. 377–382.
[124] Chillara, V. S. C., and Dapino, M. J., 2017, "Mechanically-Prestressed Bistable Composite Laminates With Weakly Coupled Equilibrium Shapes," Compos. Part B: Eng., **111**, pp. 251–260.
[125] Chillara, V. S. C., and Dapino, M. J., 2018, "Stability Considerations and Actuation Requirements in Bistable Laminated Composites," Compos. Struct., **184**, pp. 1062–1070.
[126] Chillara, V. S. C., and Dapino, M. J., 2017, "Bistable Morphing Composites With Selectively Pre-Stressed Laminae," Proc. SPIE, **10165**, p. 101650Y.
[127] Daynes, S., and Weaver, P. M., 2013, "Stiffness Tailoring Using Prestress in Adaptive Composite Structures," Compos. Struct., **106**, pp. 282–287.
[128] Emam, S. A., and Inman, D. J., 2015, "A Review on Bistable Composite Laminates for Morphing and Energy Harvesting," ASME Appl. Mech. Rev., **67**(6), p. 060803.
[129] Bilgen, O., Erturk, A., and Inman, D. J., 2010, "Analytical and Experimental Characterization of Macro-Fiber Composite Actuated Thin Clamped-Free Unimorph Benders," ASME J. Vib. Acoust., **132**(5), p. 051005.
[130] Lang, R. J., Tolman, K. A., Crampton, E. B., Magleby, S. P., and Howell, L. L., 2018, "A Review of Thickness-Accommodation Techniques in Origami-Inspired Engineering," ASME Appl. Mech. Rev., **70**(1), p. 010805.
[131] Wilding, S. E., Howell, L. L., and Magleby, S. P., 2012, "Introduction of Planar Compliant Joints Designed for Combined Bending and Axial Loading Conditions in Lamina Emergent Mechanisms," Mech. Mach. Theory, **56**, pp. 1–15.
[132] Boncheva, M., and Whitesides, G. M., 2005, "Templated Self-Assembly: Formation of Folded Structures by Relaxation of Pre-Stressed, Planar Tapes," Adv. Mater., **17**(5), pp. 553–557.
[133] Chillara, V. S. C., and Dapino, M. J., 2018, "Stress-Biased Laminated Composites for Smooth Folds in Origami Structures," Mater. Res. Express, **6**(2), p. 025703.
[134] Daynes, S., Trask, R. S., and Weaver, P. M., 2014, "Bio-Inspired Structural Bistability Employing Elastomeric Origami for Morphing Applications," Smart Mater. Struct., **23**(12), p. 125011.
[135] Li, S., and Wang, K. W., 2015, "Fluidic Origami With Embedded Pressure Dependent Multi-Stability: A Plant Inspired Innovation," J. R. Soc. Interface, **12**(111), p. 20150639.
[136] Hanna, B. H., Lund, J. M., Lang, R. J., Magleby, S. P., and Howell, L. L., 2014, "Waterbomb Base: A Symmetric Single-Vertex Bistable Origami Mechanism," Smart Mater. Struct., **24**(10), p. 105031.
[137] Martinez, R. V., Fish, C. R., Chen, X., and Whitesides, G. M., 2012, "Elastomeric Origami: Programmable Paper-Elastomer Composites as Pneumatic Actuators," Adv. Funct. Mater., **22**(7), pp. 1376–1384.
[138] Lan, X., Liu, Y., Lv, H., Wang, X., Leng, J., and Du, S., 2009, "Fiber Reinforced Shape-Memory Polymer Composite and Its Application in a Deployable Hinge," Smart Mater. Struct., **18**(2), p. 024002.
[139] Felton, S., Tolley, M., Demaine, E., Rus, D., and Wood, R., 2014, "A Method for Building Self-Folding Machines," Science, **345**(6197), pp. 644–646.
[140] Tolley, M. T., Felton, S. M., Miyashita, S., Aukes, D., Rus, D., and Wood, R. J., 2014, "Self-Folding Origami: Shape Memory Composites Activated by Uniform Heating," Smart Mater. Struct., **23**(9), p. 094006.
[141] Peraza-Hernandez, E., Hartl, D., Galvan, E., and Malak, R., 2013, "Design and Optimization of a Shape Memory Alloy-Based Self-Folding Sheet," ASME J. Mech. Des., **135**(11), p. 111007.
[142] Hawkes, E., An, B., Benbernou, N. M., Tanaka, H., Kim, S., Demaine, E. D., Rus, D., and Wood, R. J., 2010, "Programmable Matter by Folding," Proc. Natl. Acad. Sci., **107**(28), pp. 12441–12445.
[143] Koh, J.-S., Kim, S.-R., and Cho, K.-J., 2014, "Self-Folding Origami Using Torsion Shape Memory Alloy Wire Actuators," ASME Paper No. DETC2014-34822.
[144] von Lockette, P., and Sheridan, R., 2013, "Folding Actuation and Locomotion of Novel Magneto-Active Elastomer (MAE) Composites," ASME Paper No. SMASIS2013-3222.
[145] Ahmed, S., Lauff, C., Crivaro, A., McGough, K., Sheridan, R., Frecker, M., von Lockette, P., Ounaies, Z., Simpson, T., Lien, J.-M., and Strzelec, R., 2013, "Multi-Field Responsive Origami Structures: Preliminary Modeling and Experiments," ASME Paper No. DETC2013-12405.
[146] Ahmed, S., Ounaies, Z., and Arrojado, E. A. F., 2017, "Electric Field-Induced Bending and Folding of Polymer Sheets," Sens. Actuators. A, **260**, pp. 68–80.
[147] Felton, S. M., Tolley, M. T., Shin, B., Onal, C. D., Demaine, E. D., Rus, D., and Wood, R. J., 2013, "Self-Folding With Shape Memory Composites," Soft Matter, **9**(32), pp. 7688–7694.
[148] Peel, L. D., and Jensen, D. W., 2000, "Nonlinear Modeling of Fiber-Reinforced Elastomers and the Response of a 'Rubber Muscle' Actuator," 158th Fall Technical Meeting of the Rubber Division, Cincinnati, OH, Oct. 17–20, Paper No. 30.
[149] Hamamoto, A., and Hyer, M. W., 1987, "Non-Linear Temperature-Curvature Relationships for Unsymmetric Graphite-Epoxy Laminates," Int. J. Solids Struct., **23**(7), pp. 919–935.
[150] Mattioni, F., Weaver, P. M., and Friswell, M. I., 2009, "Multistable Composite Plates With Piecewise Variation of Lay-Up in the Planform," Int. J. Solids Struct., **46**(1), pp. 151–164.
[151] Peraza Hernandez, E. A., Hartl, D. J., Akleman, E., and Lagoudas, D. C., 2016, "Modeling and Analysis of Origami Structures With Smooth Folds," Comput.-Aided Des., **78**, pp. 93–106.
[152] Reddy, J. N., 1997, *Mechanics of Laminated Composite Plates: Theory and Analysis*, CRC Press, Boca Raton, FL.

[153] Dano, M.-L., and Hyer, M. W., 2003, "SMA-Induced Snap-Through of Unsymmetric Fiber-Reinforced Composite Laminates," Int. J. Solids Struct., **40**(22), pp. 5949–5972.
[154] Ogden, R. W., 1972, "Large Deformation Isotropic Elasticity-on the Correlation of Theory and Experiment for Incompressible Rubberlike Solids," Proc. R. Soc. London A: Math., Phys. Eng. Sci., **326**(1567), pp. 565–584.
[155] Gibson, L. J., and Ashby, M. F., 1999, *Cellular Solids: Structure and Properties*, Cambridge University Press, Cambridge, UK.
[156] Philen, M., Shan, Y., Wang, K.-W., Bakis, C., and Rahn, C., 2007, "Fluidic Flexible Matrix Composites for the Tailoring of Variable Stiffness Adaptive Structures," AIAA Paper No. 2007-1703.
[157] Dano, M.-L., and Hyer, M. W., 1996, "The Response of Unsymmetric Laminates to Simple Applied Forces," Mech. Compos. Mater. Struct., **3**(1), pp. 65–80.
[158] Schlecht, M., and Schulte, K., 1999, "Advanced Calculation of the Room-Temperature Shapes of Unsymmetric Laminates," J. Compos. Mater., **33**(16), pp. 1472–1490.
[159] Betts, D. N., Salo, A. I. T., Bowen, C. R., and Kim, H. A., 2010, "Characterisation and Modelling of the Cured Shapes of Arbitrary Layup Bistable Composite Laminates," Compos. Struct., **92**(7), pp. 1694–1700.
[160] Hufenbach, W., Gude, M., and Kroll, L., 2002, "Design of Multistable Composites for Application in Adaptive Structures," Compos. Sci. Technol., **62**(16), pp. 2201–2207.
[161] Tawfik, S. A., Stefan, D. D., and Armanios, E., 2011, "Planform Effects Upon the Bistable Response of Cross-Ply Composite Shells," Compos. Part A, **42**(7), pp. 825–833.
[162] Lee, A. J., Moosavian, A., and Inman, D. J., 2017, "Control and Characterization of a Bistable Laminate Generated With Piezoelectricity," Smart Mater. Struct., **26**(8), p. 085007.
[163] Brinson, L. C., 1993, "One-Dimensional Constitutive Behavior of Shape Memory Alloys: Thermomechanical Derivation With Non-Constant Material Functions and Redefined Martensite Internal Variable," J. Intell. Mater. Syst. Struct., **4**(2), pp. 229–242.
[164] Diaconu, C. G., Weaver, P. M., and Arrieta, A. F., 2009, "Dynamic Analysis of Bi-Stable Composite Plates," J. Sound Vibr., **322**(4–5), pp. 987–1004.
[165] Gigliotti, M., Wisnom, M. R., and Potter, K. D., 2004, "Loss of Bifurcation and Multiple Shapes of Thin [0/90] Unsymmetric Composite Plates Subject to Thermal Stress," Compos. Sci. Technol., **64**(1), pp. 109–128.
[166] Potter, K., Weaver, P., Seman, A. A., and Shah, S., 2007, "Phenomena in the Bifurcation of Unsymmetric Composite Plates," Compos. Part A: Appl. Sci. Manuf., **38**(1), pp. 100–106.
[167] Cantera, M. A., Romera, J. M., Adarraga, I., and Mujika, F., 2014, "Modelling of [0/90] Laminates Subject to Thermal Effects Considering Mechanical Curvature and Through-the-Thickness Strain," Compos. Struct., **110**, pp. 77–87.
[168] Pirrera, A., Avitabile, D., and Weaver, P. M., 2010, "Bistable Plates for Morphing Structures: A Refined Analytical Approach With High-Order Polynomials," Int. J. Solids Struct., **47**(25–26), pp. 3412–3425.
[169] Berbinau, P., Soutis, C., and Guz, I. A., 1999, "Compressive Failure of 0° Unidirectional Carbon-Fibre-Reinforced Plastic (CFRP) Laminates by Fibre Microbuckling," Compos. Sci. Technol., **59**(9), pp. 1451–1455.
[170] Murphey, T., Meink, T., and Mikulas, M., 2001, "Some Micromechanics Considerations of the Folding of Rigidizable Composite Materials," AIAA Paper No. 2001-1418.
[171] López Jiménez, F., and Pellegrino, S., 2012, "Folding of Fiber Composites With a Hyperelastic Matrix," Int. J. Solids Struct., **49**(3–4), pp. 395–407.
[172] Francis, W., Lake, M., and Mayes, J. S., 2006, "A Review of Classical Fiber Microbuckling Analytical Solutions for Use With Elastic Memory Composites," AIAA Paper No. 2006-1764.